TECHNIQUES FOR ESTIMATING SPACE STATION AERODYNAMIC CHARACTERISTICS

Richard E. Thomas

Texas A&M Research Foundation
Box 3578
College Station, TX 77843

July 1, 1989 - August 31, 1992

NATIONAL AERONAUTICS AND SPACE ADMINISTRATION
Lyndon B. Johnson Space Center
Houston, TX

NAG 9-386

THE EFFECT OF MULTIPLY REFLECTED MOLECULES IN FREE MOLECULE FLOW OVER A GENERAL BODY

A Thesis

by

GORDON LEE POWELL, JR.

Submitted to the Office of Graduate Studies of
Texas A&M University
in partial fulfillment of the requirements for the degree of

MASTER OF SCIENCE

May 1993

Major Subject: Aerospace Engineering

THE EFFECT OF MULTIPLY REFLECTED MOLECULES IN FREE MOLECULE FLOW OVER A GENERAL BODY

A Thesis

by

GORDON LEE POWELL, JR.

Approved as to style and content by:

Richard E. Thomas
(Chair of Committee)

Leland A. Carlson
(Member)

Mario A. Colaluca
(Member)

Walter E. Haisler
(Head of Department)

May 1993

ABSTRACT

The Effect of Multiply Reflected Molecules

in Free Molecule Flow Over a General Body. (May 1993)

Gordon Lee Powell, Jr., B.S., Texas A&M University

Chair of Advisory Committee: Dr. Richard E. Thomas

A method was devised and calculations were performed to determine the effects of reflected molecules on the aerodynamic force and moment coefficients for a body in free molecule flow. A procedure was developed for determining the velocity and temperature distributions of molecules reflected from a surface of arbitrary momentum and energy accommodation. A system of equations, based on momentum and energy balances for the surface, incident, and reflected molecules, was solved by a numerical optimization technique. The minimization of a "cost" function, developed from the set of equations, resulted in the determination of the defining properties of the flow reflected from the arbitrary surface. The properties used to define both the incident and reflected flows were: average temperature of the molecules in the flow, angle of the flow with respect to a vector normal to the surface, and the molecular speed ratio. The properties of the reflected flow were used to calculate the contribution of multiply reflected molecules to the force and moments on a test body in the flow. The test configuration consisted of two flat plates joined along one edge at a right angle to each other. When force and moment coefficients of this 90° concave wedge were compared to results that did not include multiple reflections, it was found that multiple reflections could nearly double lift and drag coefficients, with nearly a 50% increase in pitching moment for cases with specular or

nearly specular accommodation. The cases of diffuse or nearly diffuse accommodation often had minor reductions in axial and normal forces when multiple reflections were included. There were several cases of intermediate accommodation where the addition of multiple reflection effects more than tripled the lift coefficient over the convex technique.

To my parents, for all the support you have given me over the years for everything that I wanted to do; and to friends and roommates for the friendship, encouragement, and entertainment you have provided the past few years.

In memory of my good friend, Brian Harder (Oct 12, 1962 - Mar 22, 1993).

ACKNOWLEDGMENT

The author would like to thank Mr. Steve Fitzgerald, whose ideas and initial work started this project in motion. Thanks, also, to the rest of the people at NASA Johnson Space Center, who funded the research project, and assisted with the Orbital Aerodynamics Computer Program. Thanks are also due to the faculty and staff of the Aerospace Engineering Department, as well as fellow graduate students who offered support and advice. Thanks to Mr. Maurice Griffin, who assisted in the early stages of this research. Special thanks go to Dr. Richard Thomas for his immense patience and stalwart support.

TABLE OF CONTENTS

LIST OF TABLES

LIST OF FIGURES

LIST OF SYMBOLS

A, A_{ref}	reference area of a surface subshape
c	thermal velocity of molecule
C_A	axial force coefficient
C_D	drag force coefficient
C_L	lift force coefficient
C_{MP}	pitching moment coefficient
C_{MR}	rolling moment coefficient
C_{MY}	yawing moment coefficient
C_N	normal force coefficient
C_Y	side force coefficient
E	flux of energy across an element of surface area
f	Maxwellian distribution, fraction of diffusely reflecting molecules
F_1	equation based on conservation of tangential momentum
F_2	equation based on conservation of normal momentum
F_3	equation based on conservation of energy
J	objective function for the optimization of conservation equations
k	Boltzman's constant (gas constant per molecule)
m	mass of gas molecule
n	number density of gas molecules
$\dot{N}$	particle flux per unit area per unit time
P	component of momentum normal to surface due to flux of gas molecules

R	gas constant per unit mass
S	speed ratio, mass velocity divided by thermal velocity
T	temperature
U	macroscopic mass velocity
V	velocity
x,y,z	orthogonal coordinate system for each individual subshape
X,Y,Z	orthogonal global coordinates for entire body and flowfield
α	energy accommodation coefficient
γ	ratio of specific heats for a gas
$\hat{\eta}$	unit vectors in principle coordinate directions
θ	angle between a velocity vector and the vector normal to the surface
λ	mean free path in the gas
ξ	total velocity, sum of mass and thermal velocities
σ_n,σ_τ	normal and tangential momentum accommodation coefficients
τ	tangential momentum due to flux of gas molecules
ψ	cosine of the angle between the normal and velocity vectors

subscripts

i,∞	incident flow
INT	internal, for internal modes of energy
mp	most probable
r	reflected flow
w	wall conditions

INTRODUCTION

Satellite and aerodynamics are two words that many people would not usually associated with each other. In designing satellites, aerodynamics is not generally important for determining the structure or configuration of the craft. In the highly rarefied gas present at orbital altitudes, the actual forces exerted on a satellite are orders of magnitude less than those experienced by aircraft. However, due to the much longer time of flight for satellites compared to a typical aircraft mission, the cumulative effect of the forces over time is of great concern.

Concern about the composition and density of the upper atmosphere and rarefied gas dynamics preceded the space age as aircraft and rockets flew higher and faster. With the advent of the space age, there was a desire for a better understanding of satellite aerodynamics because "it will permit accurate predictions of the expected impact locations of heavy or dangerous payloads, so that attempts can be made to divert them from impact areas where damage could result or areas that would be embarrassing."[1] The Rand Corporation study of orbital decay was initiated soon after a 21 pound chunk of iron and steel, a portion of Sputnik IV, fell on a street corner in Manitowoc, Wisconsin in September of 1962. Today, more important than concerns about debris from reentering spacecraft, the aerodynamic forces and moments on an orbiting body are of concern for the designers of the craft for a number of other reasons. The primary motivations are: sizing the attitude stabilization and control systems, a need to determine orbital re-boost, determining propellant requirements between service visits, sizing a gyro-stabilization

---

Journal model is *AIAA Journal.*

system, and calculating the acceleration environment for micro-gravity experiments. The space station program, designing Freedom, has many of these concerns.

The flight regime of these orbiting vehicles is known as free molecular flow (FMF). Free molecular flow is the regime of rarefied gas dynamics where collisions between molecules in the flow can be ignored when compared to the frequency of collisions between the flow and the body immersed in the flow. Essentially, the particles reflected from a surface do not interact with particles in the freestream and therefore do not affect the incoming flow as they do in continuum flows.

Several aspects of satellite aerodynamics need to be investigated more thoroughly in order to better predict forces and moments on a craft. Long the primary difficulty of satellite aerodynamics, modeling the atmosphere at orbital altitudes has become more tractable with the availability of more accurate data. The next logical area to seek improvement is in the techniques for estimating the force and moment coefficients on a body in the atmosphere at orbital altitude. This is especially important with the increasing complexity of satellite configurations such as the space station Freedom, with its truss structure and numerous large panels.

It is no longer feasible to model all vehicle configurations as if they were simple convex bodies. Convex bodies are easiest to model in free molecule flow since the transfer of momentum and energy of the impinging particles can be calculated and then the particles can be forgotten about. The traditional methods for calculating the aerodynamic forces and moments in free molecule flow could still be adequate if the body being studied is configured as a convex surface. A concave surface, on the other hand, allows the impinging freestream molecules to reflect off one portion of the body and possibly strike

the body again. Each interaction of a gas particle and the surface contributes to the total force and moment on the body.

Background

In any study of free molecule flow of gas, there are three main flow parameters that should be kept in mind. One of the most important parameters is the Knudsen number, Kn, based on the mean free path. The mean free path is the average distance that a molecule travels between collisions with other particles in the gas. The Knudsen number is defined to be λ/l, where λ is the mean free path, and l is some characteristic length. For interior flows, the characteristic dimension is often taken to be the diameter of the channel. In the case of exterior flows, the characteristic length may be the overall length of the body about which the flow is being studied. Another important parameter is the molecular speed ratio, S. The speed ratio is similar to the Mach number, but applicable to the molecular flow of gases. S is the ratio of the macroscopic mass velocity of the gas to the thermal velocity of the gas particles. The third parameter to be considered is the temperature ratio. T_w/T_i is the ratio of the body wall temperature to the incident freestream temperature.

The mean free path, so critical for defining the free molecule flow regime, is related to the atmospheric density. For a constant gas temperature and composition, the mean free path is inversely related to density. Like density, the variation of mean free path in the atmosphere can be crudely modeled as exponential with altitude. At standard conditions, the mean free path is about 6×10^{-6} cm, and at orbital altitudes of 400 km it is roughly 1×10^{4} m.

The field of gas dynamics is further subdivided by consideration of the Knudsen number. There are three flow regimes that are generally considered. For cases where the Knudsen number is much less than unity, ranging from the inviscid limit of 0.0 up to about 0.1, the flow is in the continuum region. The continuum region is that flow regime that encompasses "normal" aerodynamics. The gas behaves as a continuum and it is very difficult to evaluate the effects of individual gas particles or molecules. When the Knudsen number is near 1.0, aerodynamic processes are termed transition or slip flows. Under those circumstances, the normal boundary layer assumption of zero velocity at the body surface may no longer apply. In this slip flow, the boundary layer is still in existence, but the gas velocity at the wall is greater than zero. The third regime, and the one of interest in the present work, is free molecule flow. Free molecule flow is generally defined as a flow with a Knudsen number much greater than 1.0. Because the incident and reflected flow do not interact with each other, the total flow may be analyzed by a superposition of the two streams.

Since all the momentum and energy transfer occurs directly on the body surface, it is necessary to know how a particle interacts with a surface. Accommodation coefficients are commonly used to describe the fraction of momentum and energy transferred to a body by a colliding molecule. The forms of the energy, normal momentum, and tangential momentum accommodation coefficients to be used in this study are:

$$\alpha = \frac{E_i - E_r}{E_i - E_w}$$

$$\sigma_n = \frac{P_i - P_r}{P_i - P_w} \qquad (1)$$

$$\sigma_\tau = \frac{\tau_i - \tau_r}{\tau_i}$$

where E_i, P_i, and τ_i are fluxes on the surface of the incident energy, tangential momentum, and normal momentum. E_r, P_r, and τ_r are the fluxes at the surface due to reemitted molecules, and E_w, P_w are the fluxes of molecules that are in Maxwellian equilibrium with the wall.[2]

For modeling the rarefied gas environment, the distribution of velocities is commonly considered to be Maxwellian[3]:

$$f = \frac{n}{(2\pi RT)^{3/2}} \exp\left[\frac{-\underline{c}^2}{2RT}\right] \qquad (2)$$

The freestream flow is assumed to be a drifting Maxwellian gas, striking a surface of arbitrary (but known) accommodation α, σ_n, σ_τ:

$$f_i = \frac{n_i}{(2\pi RT_i)^{3/2}} \exp\left[\frac{-(\underline{\xi} - \underline{U}_i)^2}{2RT_i}\right] \qquad (3)$$

Where the velocities of the molecules, ξ, are considered to be a superposition of the macroscopic mass velocity, U, and the random thermal velocity, c.

$$\underline{\xi}_i = (\psi_i U_i + c_1)\hat{\eta}_1 + (\phi_i U_i + c_2)\hat{\eta}_2 + (\theta_i U_i + c_3)\hat{\eta}_3$$
$$\underline{\xi}_r = (-\psi_r U_r + c_1)\hat{\eta}_1 + (\phi_r U_r + c_2)\hat{\eta}_2 + (\theta_r U_r + c_3)\hat{\eta}_3 \quad (4)$$

In addition, the flow reemitted from the surface is also assumed to take on a drifting Maxwellian distribution.

$$f_r = \frac{n_r}{(2\pi R T_r)^{3/2}} \exp\left[\frac{-(\underline{\xi} - \underline{U}_r)^2}{2RT_r}\right] \quad (5)$$

Previous Work

The study of free molecule flow, although it has numerous high-tech and modern applications, is by no means a new field of study. Some of the earliest works involving modern rarefied gas flow were carried out by James Clerk Maxwell and his contemporaries. Maxwell was the first to investigate gas flows with large mean free paths and one of the first to put an understanding of rarefied flows of gas to work, explaining the effects of Crooke's radiometer and rarefied gas flows in capillary tubes. Perhaps the most important assumption he made with regard to free molecule flow was to break up the reflected flow from a surface into two components. A fraction, f, of the particles are reflected in a manner that transfers all of their tangential momentum to the surface, so the reflected flow would not have any net velocity parallel to the surface. The remaining fraction, 1-f, reflects in a mirror-like fashion, transferring only normal momentum to the

surface and not affecting the component of velocity parallel to the surface.[4]

The two components of flow that are usually considered today are specular and diffuse reflection. In specular reflection, the incident flow is unaffected in the direction parallel to the surface and the direction of the flow perpendicular to the surface is changed in direction only. The magnitude of velocity perpendicular to the surface is unchanged. For diffuse reflection, the incident flow is completely accommodated to the surface conditions. The reflected particles leave the surface in a uniform distribution with no net motion parallel to the surface.

Knudsen was also an early contributor in the field. In L.B. Loeb's book, *The Kinetic Theory of Gases*, 1934, he references work done by M. Knudsen, published in 1909, on the effusion of gases through a hole in a thin diaphragm.[5] In that work, he developed the cosine distribution for the direction of molecular flow emitting from a point. Knudsen is also attributed by Sänger as having developed the idea of diffuse reflection.[6] In the same paper, the idea of mirror or specular reflection is cited as being due to Newton. Sänger was the first to detail the free molecule transfer of energy of the internal degrees of freedom of diatomic molecules.

Many of the early studies of free molecular processes were for flows at low speed and for internal flow configurations. The results of this work were applied in vacuum processes and to flows through ducts and orifices.

A.F. Zahm coined the term Superaerodynamics to refer to flight in conditions of high Mach number, high altitude and hence low density, and was one of the first to consider the high speed molecular flows that would be found by advanced vehicles in high altitude flight.[7] Sänger, in his paper referenced above, was also one of the early

investigators of high speed rarefied gas flows. His work included calculation of the drag of a normally inclined flat plate in a flow of finite speed ratio.

However, most of the advances in free molecule flow at high speeds were made after World War II. This was the period of the "perfection" of the rocket engine, and the beginning of an era in which free molecule flow became of practical concern. Superaerodynamics was no longer just in the realm of the theorist. Tsien's 1946 paper considered the molecular flow at large freestream Mach number over an inclined flat plate. As Tsien noted, the greatest simplification of free molecule flow over continuum methods was that "one need not consider the distortion of the Maxwellian distribution due to the collision of the re-emitted molecules with the molecules in the stream."[8]

The introduction of a thermal accommodation coefficient is attributed to Smoluchowsky and Knudsen. The coefficient is defined by:

$$\alpha = \frac{dE_i - dE_r}{dE_i - dE_w}$$

where dE_i and dE_r are energy fluxes incident on and reemitted per unit time from a differential element of area. The value of dE_w is the flux of energy corresponding to a flow of reemitted molecules with a Maxwellian distribution with a temperature, T_w, equal to the wall temperature. In a slight change from Maxwell's method, Schaaf and Chambré introduce both a tangential and normal momentum accommodation coefficient in parallel to the energy accommodation, since a single parameter, like f, may not be sufficient to describe the reflection process adequately.[9]

$$\sigma = \frac{\tau_i - \tau_r}{\tau_i - \tau_w}, \quad (\tau_w = 0)$$

$$\sigma' = \frac{p_i - p_r}{p_i - p_w}$$

where τ and p are the tangential and normal components of momentum.

Numerous investigations were carried out in the post war period, but nearly all the work involved flow over bodies that are convex. Schaaf and Chambré, in "Flow of Rarefied Gases", provide a table of works exploring flow around plates, cylinders, spheres, cones, ogives, ellipsoids, and composite bodies. Sentman produced a very thorough paper that very clearly demonstrated how to calculate the force and moment coefficients on a complex body made up of elements including flat plates, circular cylinders, cone frustums, and spherical segments.[10] He notes that his equations account for shielding such as the back surface of a cylinder by the front surface, but not shielding of one element by another, so that care must be taken in their application.

Sentman's work at Lockheed was followed by the development of a computer program at Lockheed Missiles & Space Company's Huntsville Research & Engineering Center. This orbital aerodynamics program, which added the ability to account for mutual molecular shadowing, used Sentman's equations to allow the calculation of the aerodynamic forces and moments on a complex vehicle shapes.[11] It is still in use today, and this research endeavors to expand the accuracy and utility of the program.

It was not until the late 1950's and early 1960's that external flow over concave shapes began to appear in the literature with any regularity. Ira Cohen and Moustafa Chahine were among the first to tackle the problem. Cohen investigated the flow into an

open hemisphere with diffuse reflection of molecules.[12] Chahine studied specular reflection and partial accommodation in an infinite cylindrical surface and in a spherical segment.[13]

Additional work on the free molecule flow over a general concave body appears in Kogan and also in Patterson. Kogan presents a thorough but nonapplied derivation of the integral equations for flow over a concave surface and includes some data from other investigations.[14] Patterson also touches on the problem of concave surfaces, but limits his investigation to the application of rarefied flow in pipes.[15]

Bird considers flows with multiple reflection and states their importance to external flows past bodies of complex geometry. He notes that the Fredholm integral equation of the second kind that arises in the solution of this problem is necessarily solved numerically. He does discuss in detail the application of the test-particle Monte Carlo method to flows around geometries that are too difficult to calculate analytically. He demonstrates the Monte Carlo method for a circular tube flux problem.[16]

Koppenwallner also included some aspects of flow over concave surfaces in his work. He chose not to investigate the full effects of multiple reflections on a concave surface, but did include the effect he calls "screening" on concave elements. His results are exact for the case where $T_w/T_\infty = 0$ and $S_w = \infty$, but can be used as an approximation for cases with $T_w/T_\infty < 1$ and $S_w >> 1$.[17] A note should be made about the difference of shielding and screening. Shielding is when a portion of the body is positioned directly between one part of the body and the direction of the mass velocity vector. Recognizing that the incoming flow has a distribution of directions based on the thermal velocity of the gas, shielding is when a portion of the body blocks flow to another part of the body from

directions other than the mass velocity.

Objectives

The calculation of the effects of multiple reflections for a general body in free molecular flow is a problem that has been identified and considered for many years. The problem has been found to be difficult in both the analytical and numerical fields. Analytic solutions for the problem involving fairly simple geometries have been found by several researchers. However, an analytic closed form solution for a general geometric body has not been developed, since the integration over an arbitrary body is difficult or impossible. Previous works have concentrated on simple geometries such as L-shaped or flapped flat plates, hollow semicylinders, and hollow hemispheres.

In addition to difficulties resulting from geometry, most works assume specific values for the surface accommodation coefficients. The most common assumptions are diffuse reflection, followed by specular reflection. Accommodation coefficients have values of 1.0 for diffuse reflection, indicating that the molecules are reemitted from the surface with a Maxwellian distribution of speeds but no mass velocity parallel to the surface. The molecules have a mean temperature equal to that of the wall. The assumption of specular reflection indicates that no energy accommodation takes place and that tangential momentum of the particles is not changed. The normal momentum does not change in magnitude but the direction is reversed. For specular reflections, all three accommodation coefficients are defined to be zero.

Another difficulty encountered when dealing with the problem of multiply reflected

molecules is the question of how the particles interact with a surface, or more precisely, the behavior of the particles leaving a surface after impingement. When convex bodies are considered, the only concern is the momentum and energy transferred to the surface. There is no need to know the eventual disposition of the reflected particles. However, when including the effects of reflected particles on concave bodies, the momentum and energy properties of the reflected particles are critical because it is possible for those molecules to strike a secondary surface and impart further momentum and energy transfer to the surface.

Once the behavior of the reflected particles is determined, a way must be developed to implement that information. For a general concave body, the flow reflected from a surface element may strike the body again in another location. Any element on the body may see a combination of previously reflected and freestream flows striking the surface. A problem when considering multiple reflections is that some particles may strike the surface only once, while others may strike the surfaces twice or even many times.

In this research, a method for numerically determining the distribution of reflected momentum and energy for a general body with arbitrary accommodation is presented. The ability to calculate the reflected distributions, and hence possibly the secondary collisions, leads to a more physically "exact" method of calculating the force and moment coefficients on an arbitrary body with arbitrary values of the accommodation coefficients. An existing computer program, the Lockheed Orbital Aerodynamics Computer Program, is updated to include the effects of multiple reflections in the calculation of free molecule aerodynamic forces and moments.

DETERMINING THE REFLECTED FLOW PROPERTIES

The first objective was to determine the properties that defined the flow of reflected particles from a surface. The initial work and ideas for the task were produced by Mr. Steve Fitzgerald under the auspices of a NASA Johnson Space Center program to improve the aerodynamic modeling of the space station Freedom. Fitzgerald realized that the three expressions defining the momentum and energy accommodation coefficients were expressions of the conservation of normal and tangential momentum and energy. The coefficients were defined as:

$$\alpha = \frac{E_i - |E_r|}{E_i - |E_w|} \quad , \qquad \sigma_n = \frac{P_i - |P_r|}{P_i - |P_w|} \quad , \qquad \sigma_\tau = \frac{\tau_i - |\tau_r|}{\tau_i} \tag{6}$$

The equations were simply rearranged and set equal to zero such as:

$$\begin{aligned} 0 &= (1-\sigma_\tau)\tau_i - |\tau_r| \\ 0 &= (1-\sigma_n)P_i + \sigma_n|P_w| - |P_r| \\ 0 &= (1-\alpha)E_i + \alpha|E_w| - |E_r| \end{aligned} \tag{7}$$

By substituting the gas kinetic expressions for each of the fluxes into equations (7) above, a system of three equations was produced. A more detailed explanation and derivation is shown in Appendix A. Given defining information about the incident flow upon the surface such as T_i, S_i, ψ_i, and complete knowledge of the surface, geometry and accommodation coefficients, the system becomes one of three equations with three unknowns. Unfortunately, because of non-linearities like the error function, the system cannot be solved by analytic methods.

However, because it is possible to put fairly definite and reasonable bounds on the unknowns and because it is possible to make a fairly good initial guess at a solution, a simply constrained, non-linear optimization technique is readily applicable. Setting each of the equations equal to F_1, F_2, or F_3 respectively:

$$\begin{aligned} F_1 &= 0 = (1-\sigma_\tau)\tau_i - |\tau_r| \\ F_2 &= 0 = (1-\sigma_n)P_i + \sigma_n|P_w| - |P_r| \\ F_3 &= 0 = (1-\alpha)E_i + \alpha|E_w| - |E_r| \end{aligned} \tag{8}$$

It is necessary to form an objective function from F_1, F_2, and F_3 that can be minimized:

$$J = \tfrac{1}{2}\left[F_1^2 + F_2^2 + F_3^2\right] \tag{9}$$

To insure that each of the individual equations, F, independently approach zero without simply summing to zero, each term in the cost function is squared.

The objective or "cost" function can be solved by a nonlinear optimization technique. J can be minimized given the input values of σ_n, σ_τ, α, T_i, ψ_i, S_i, γ, and T_w. These quantities are known from material properties, atmospheric data and the geometry of the problem. The constraints are simple bounds on the variables T_r, ψ_r, and S_r. T_r is bounded by the lowest and highest of the incident and wall temperatures. ψ_r is bounded to keep the reflected velocity directed out of the surface, and not into it. S_r is bounded by zero and the incident speed ratio, S_i, for most usual cases of accommodation.

A commercial Fortran optimization routine was utilized to take advantage of an existing and reliable optimization scheme. The double precision routine will minimize a

function of N variables subject to bounds on the variables using a quasi-Newton method and a user-supplied gradient. Optionally, a different commercial routine may be used for the optimization. This routine will also minimize a function of N variables subject to bounds on the variables using a modified Newton method and a user-supplied Hessian.

The initial guesses for optimization are simple functions of the freestream conditions and the accommodation coefficients. The purpose of a set of calculated initial guesses is to provide a beginning point for the optimization search that is closer to the solution than, say, the incident conditions. A set of guesses that is deemed to at least approximate a likely solution will possibly help avoid local minima in the search for a global minimum and reduce the number of search steps needed. The set of initial guesses that seemed to provide the most consistent results for all combinations of accommodation was:

$$\begin{aligned} T_{guess} &= T_i + \alpha(T_w - T_i) \\ \psi_{guess} &= \alpha + \psi_i(1-\alpha) \\ S_{guess} &= (1-\alpha) S_i \end{aligned} \tag{10}$$

Successful minimization of the cost function results in the desired values of ψ_r, S_r, and T_r necessary for the determination of the distribution of the stream reflected from a surface. When a global minimum is found, the value of the cost function should be very near zero. For the cases run in this investigation, the cost function at the location of a solution was often in the neighborhood of 10^{-10} to 10^{-20}, although it was occasionally as large as 10^{-4}. For comparison, the cost function evaluated with the initial guesses (i.e. at the start of optimization) may be as large as 10^{4}.

Successful minimization of the cost function is not automatically assured, even with a "good" set of initial guesses. The choice of a set of accommodation coefficients to

describe a surface is not really an arbitrary matter, but a material property. So, a poor choice of accommodation coefficients may lead to a set of equations that have no solution--can not be minimized successfully. Appendix B discusses the selection of accommodation coefficients and the successful determination of the properties of the reflected flow.

APPLICATION OF MULTIPLE REFLECTIONS

Since in free molecule flow the gas molecules do not interact with one another but only with the surface, the flow of incident and reflected particles can be appraised separately and the results summed to calculate the cumulative effect. With that in mind, it was decided that the best way to compare the forces on a body with and without consideration of multiple reflections was to continue to use the Lockheed Orbital Aerodynamics Program and add the necessary sections of code to calculate the contribution from multiple reflections.

Orbital Aerodynamics Computer Program

The Orbital Aerodynamics Computer Program is a computer code written in the Fortran language that can obtain aerodynamic force and moment coefficients for any complex vehicle, symmetrical or asymmetrical, at any vehicle angle of attack or roll, or combination of both. The code handles complex vehicles by regarding each composite part (subshape) of the vehicle as a separate body. The code can handle mutual shadowing of subshapes and can model vehicles using cylinders, cones and cone frustums, circular plates and rings, rectangular plates, right-angled triangular plates, and spheres. Based on a user input mean free path for each altitude case, the Knudsen number is calculated and force and moment coefficients are calculated as required by the flow regime. Rarefied continuum flow utilizes modified Newtonian theory. The transition regime makes use of an empirical relation that was developed to approximate experimental data. The FMF regime uses the standard formulations of free molecule theory, and Sentman's equations in particular.

The FMF calculations are carried out using the general force equation:

$$\frac{dC}{dA} = \frac{1}{A_{ref}}\left\{\left[\sigma_\tau(\epsilon k+\eta t) + (2-\sigma_\eta)\gamma l\right]\left[\gamma(1+\mathrm{erf}\gamma S) + \frac{1}{S\sqrt{\pi}}\exp(-\gamma^2 S^2)\right]\right.$$
$$\left. + \frac{(2-\sigma_\eta)}{2S^2} l(1+\mathrm{erf}\gamma S) + \frac{\sigma_\eta l}{2}\sqrt{\frac{T_w}{T_i}}\left[\frac{\gamma\sqrt{\pi}}{S}(1+\mathrm{erf}\gamma S) + \frac{1}{S^2}\exp(-\gamma^2 S^2)\right]\right\}$$

where k, l, t are direction cosines between the local coordinates and the desired force direction. ϵ, γ, η are direction cosines between the local coordinates and the mass velocity vector. The contribution from the reflected particles can also use the same force calculating routines. The key is to use the correct direction cosines for the above equation. Instead of the mass velocity vector, the reflected velocity vector (determined from the optimization process) can be used.

Assumptions for Reflected Flow

Several basic assumptions were made for the modeling of the reflected flow. The most severe is that only one interaction of the reflected molecules was considered. If the reflected particle were to strike the surface and reflect again onto another part of the configuration, that effect would not be included. The test configuration was designed to make the possibility statistically insignificant, except for cases near pure diffuse reflection. However, in purely diffuse reflection, the first interaction with the surface would result in a particle having a temperature equal to the surface, and no mass velocity relative to the vehicle. Any further interactions with the surface should not be significant, especially when the wall temperature is markedly less than the incident temperature.

The parameters that were input to the OA code to define the flow regime were chosen to represent conditions in low earth orbit. For the test cases, the temperature ratio, T_w/T_i, was 0.25. The incident speed ratio, S_i, was chosen to be 7.5, and a mean free path of 10,000 units insured the applicability of free molecule flow. A value of 1.1 was chosen for the ratio of specific heats for the gas, γ. The OA code requires input of a reference radius for the calculation of the reference area. The radius used for this investigation was 0.5642, corresponding to the radius of a circle of area 1.0.

The mass velocity vector of the reflected flow was also assumed to stay in the same plane as that defined by the incident velocity and the normal to the surface, consistent with the reflection model used. By limiting the freestream velocity to the X,Y plane, the test is kept symmetrical about the X,Y plane and side force (C_Y), rolling moment (C_{MR}), and yawing moment (C_{MY}) are all held to 0.0.

Description of Test Configuration

The configuration used to test the multiple reflections code could be called a concave wedge. The model consists of two square flat plates, each with unit area, located at right angles to each other with one edge of the first plate next to one edge of the other plate. The configuration is defined to be at 0° angle of attack when the bisector of the angle between the plates is directed straight into the flow. The origin of the global coordinate system is at the center of the wedge, located at the intersection of the bisector and a segment joining the centers of the two flat plates. The global X coordinate direction is in the opposite direction of the bisector of the wedge, and the Y coordinate is "up". The

Z coordinate direction completes the right hand system by being parallel to the corner joint of the plates. Figure 1 shows the test configuration and coordinate systems. Figure 2 shows more clearly the way subshapes were used to model the concave wedge.

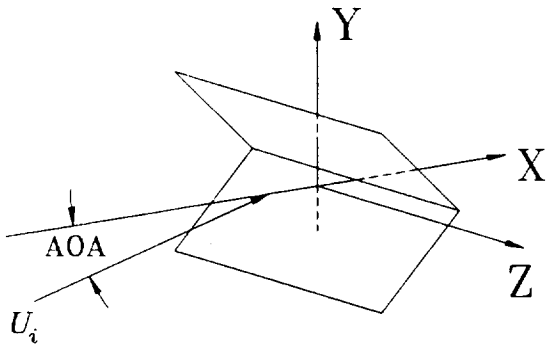

Fig. 1 Global coordinate system and axis with relation to freestream velocity vector.

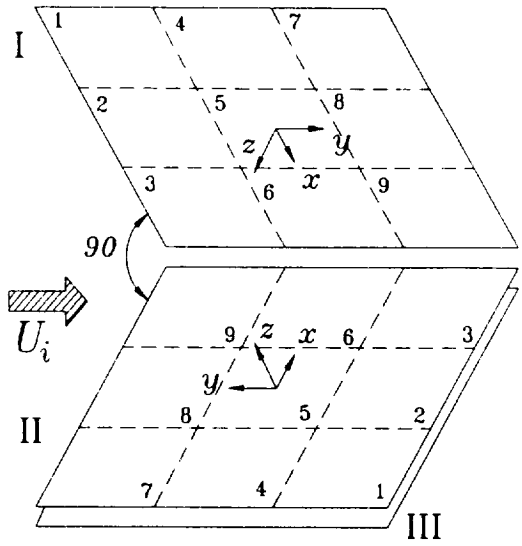

Fig. 2 90° wedge test configuration geometry and local coordinate systems with subshape and element numbering scheme.

Every surface of the configuration that is exposed to flow must have a subshape assigned to it. To model the flow over a flat plate with both sides exposed to the flow requires two rectangular subshapes: one for the top surface and one for the bottom. By restricting the investigation to a range of angles of attack from 0° to 45°, some simplification of the model takes place. Only three subshapes are required, one (plate I) on the top half of the wedge, and two (plates II and III) on the bottom half. For reasons discussed later in this report, it was not necessary to continue the range of angle of attack beyond 45°. Although it would be valid to use the concept of this work in angles of attack greater than 45°, the present means of application renders the method invalid for that range

of angles.

Each subshape is further divided into area elements for calculating force and moments. The Orbital Aerodynamics (OA) code calculates the incremental forces for each element and sums them all to give the final values of force and moment coefficients. The values calculated by the OA code are stored so that the contribution from multiple reflections may be added to them. The idea is to cycle through all elements of each subshape and determine the reflected flow from that point to every other element of the other subshapes.

There are several ways to cut down on the number of element to element cases that must be checked. First, since all the subshapes are flat or convex, it is assumed that no reflected flow from one element will strike another element on the same subshape. Second, if the element is receiving no incident flow from the freestream, then it will not send any reflected flow to other subshapes. Third, by testing the dot product of the normal vectors from two elements, it can be determined if it is physically possible for flow to go from the outer surface of one element to the outer surface of the other. Elements of flat subshapes can all share the same coordinate system, translated to the center of each element, thereby cutting down on the number of coordinate system rotations that must be calculated, as in a cylindrical or conic subshape.

Determination of Reflected Particle Flux Distribution

Since the reflected flow is defined by a direction vector away from the point of reflection, calculating the effects on a secondary element that does not lie directly on that

vector could be a difficulty. Fortunately, S. Nocilla developed a model for the re-emission of molecules from a surface in free molecule flow.[18] This re-emission law is the key to the application of multiple reflections to free molecule flow. Nocilla derived what he called the "intensity" of reflected flow in any direction from the reflective surface. The intensity is the number flux of particles in an elementary solid angle $d\Omega$ divided by the total number flux of particles emitted from an area element:

$$I_r^{(\Omega)} = \frac{N_r^{(\Omega)}}{N_r}$$

$$I_r^{(\Omega)} = \frac{\exp(-s_r^2)}{\pi\chi(\sigma_r)}\cos\Theta\,[1 + F(X_r)] \tag{12}$$

where:

$$\cos\bar{\theta}_r = \sin\theta_r \sin\Theta\cos\phi + \cos\theta_r\cos\Theta$$

$$\sigma_r = s_r\cos\theta_r$$

$$\chi(\sigma_r) = \exp(-\sigma_r^2) + \pi^{1/2}\sigma_r(1 + \operatorname{erf}\sigma_r)$$

$$X_r = s_r\cos\bar{\theta}_r$$

$$F(X_r) = X_r^2 + \pi^{1/2}(\tfrac{3}{2}X_r + X_r^3)(1 + \operatorname{erf} X_r)\exp X_r^2$$

and it follows that:

$$\int_\Omega I_r^{(\Omega)}\, d\Omega = 1$$

According to this model, the re-emitted molecules are in Maxwellian equilibrium with a translational velocity, U_r. Figure 3 shows the coordinate system for the velocities and Fig. 4 shows how the intensity could be integrated over a region in space to determine the particle flux from an elemental area to that region in space. An attraction of the Nocilla model is its simplicity. However, it is also quite accurate at predicting the reflected distributions, at least for the particle energies investigated by F. C. Hurlbut, which were used for comparison by Nocilla. The experimental results were taken from

Hurlbut's 1959 Rand report detailing the projection of nitrogen molecular beams on lithium fluoride crystals.

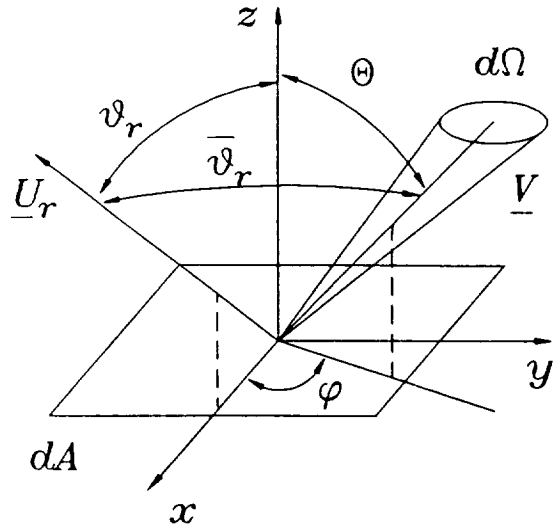

Fig. 3 Geometry used to define elementary solid angle for integration of Nocilla's intensity.

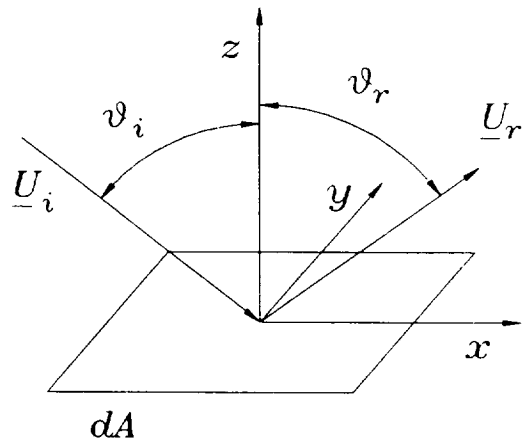

Fig. 4 Incident and reflected velocity vectors for a surface area element.

The intensity of the reflected flow was integrated over the area of each secondary element that might receive reflected flow from the primary element. A simple two dimensional quadrature integration from a commercially available math subroutine library was employed. The integration was performed in the azimuthal and elevation directions of a spherical type coordinate system.

The limits over which the intensity was integrated for each secondary element were determined by finding the four vectors from the center of the primary element to each of the corners of the secondary element. By comparing the directions of the corner vectors, two of the corners were chosen as the limits for the azimuthal integration. The limits for the elevation integration were then found as functions of the azimuthal location along the edges of the secondary element.

The force and moment routines from the original Orbital Aerodynamics Program could be used for the reflected flow as well as the freestream, with several minor differences. The correct directional cosines were calculated for the reflected flow and desired force directions. The force coefficient calculated by the routine had to be further modified by two factors: the intensity, and a geometric factor. The value of the intensity, integrated over the region in space occupied by the secondary element, is the first factor. A ratio of the primary to secondary elemental areas, each multiplied by the cosine of the angle between the normal vector and the flow direction coming into the element, is the second factor. This geometric factor accounts for the difference in cross sectional area each element presents to the flow.

These calculations produced the incremental force coefficient added by the consideration of multiply reflected molecules. The resultant incremental forces were stored and, after all elements were evaluated, were summed with the forces and moments from the convex results produced by the old code. The output portion of the code was altered to provide listings of both the convex and concave results.

RESULTS AND DISCUSSION

The free molecule flow over the concave wedge was evaluated for a speed ratio of 7.5, and a wall to incident temperature ratio of 0.25. Eight sets of accommodation values were tested, and results compared to the values calculated without consideration of multiple reflections. In addition to varying the accommodation values, several different cases were evaluated with different grid resolutions for the numerical integration.

The traditional limiting cases of specular and diffuse reflection were run with grid sizes of 2x2, 4x4, and 8x8 for the integration. The original Lockheed Orbital Aerodynamics Code provides exactly the same answers for all grid sizes when flat subshapes are used, so there is only one set of data present for the convex cases. The rest of the accommodation cases only include the values for 8x8 grid spacing.

Results for $\alpha = 0.0$, $\sigma_t = 0.0$, $\sigma_r = 0.0$

There were significant increases in the axial and drag coefficients with specular reflection that should be noted. Table 1 contains the output coefficients for the fully specular case. The axial force coefficient for the specular case increased by an amount in excess of 2.51 when the vehicle was at an angle of attack (AOA) of 0°. This was just over an 87% increase in the coefficient value from the results without multiple reflections. The effect of multiple reflections diminished with increasing angle of attack, and the results with and without multiple reflections converged at the 45° AOA case as shown in Fig. 5. Figure 6 compares the normal force coefficient for convex and concave results. There is no difference in results for the 0° AOA case, but there is an 89% increase with multiple

reflections for the 5° AOA case. The results again converge for the 45° case. At 0° AOA, the effects of grid size are the greatest. The 2x2 grid results are 2.0% higher than the 4x4 grid, and the 4x4 grid is 1.2% higher than the 8x8 grid. The different grid sizes all clearly represented the same trends.

Table 1 Force and moment coefficients for a 90° concave wedge with S_∞ = 7.5, T_w/T_∞ = 0.25, and $\alpha = \sigma_\eta = \sigma_\tau = 0.0$, 8x8 grid.

Results from Orbital Aerodynamics Code						Results with multiple reflect. effects					
AOA	C_A	C_N	C_L	C_D	C_M	AOA	C_A	C_N	C_L	C_D	C_M
0	2.8806	0	0	2.8806	0	0	5.3923	0	0	5.3923	0
5	2.8806	.4915	.2385	2.9125	.1542	5	9.2037	.9294	.4723	5.2649	.1694
10	2.8806	.968	.4531	3.005	.3038	10	4.8801	1.6841	.811	5.0984	.2907
15	2.8806	1.4152	.6214	3.1487	.4441	15	4.5467	2.2673	1.0133	4.9786	.3907
20	2.8806	1.8193	.7243	3.3291	.5709	20	4.237	2.6996	1.0876	4.9048	.4852
25	2.8806	2.1681	.7476	3.527	.6804	25	3.9492	2.9879	1.039	4.842	.5748
30	2.8806	2.4511	.6824	3.7203	.7692	30	3.6742	3.1352	.8781	4.7495	.6605
35	2.8804	2.6599	.5267	3.8851	.8347	35	3.4065	3.1497	.6262	4.597	.7438
40	2.8784	2.7896	.2867	3.9981	.8754	40	3.1408	3.0445	.3134	4.3629	.8228
45	2.8555	2.8555	0	4.0382	.8961	45	2.8558	2.8551	-.0005	4.0382	.896

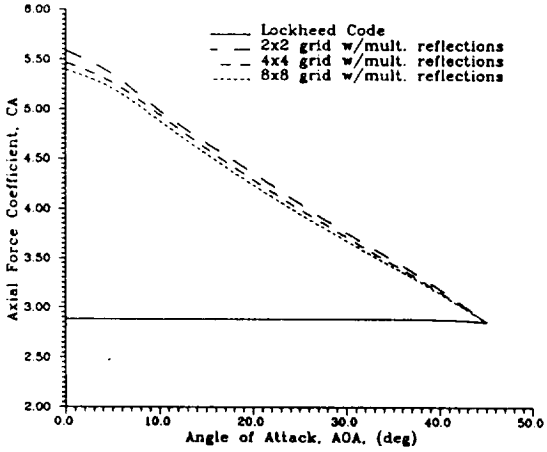

Fig. 5 Axial force coefficient for a 90° concave wedge with S_∞ = 7.5, T_w/T_∞ = 0.25, and $\alpha = \sigma_\eta = \sigma_\tau = 0$.

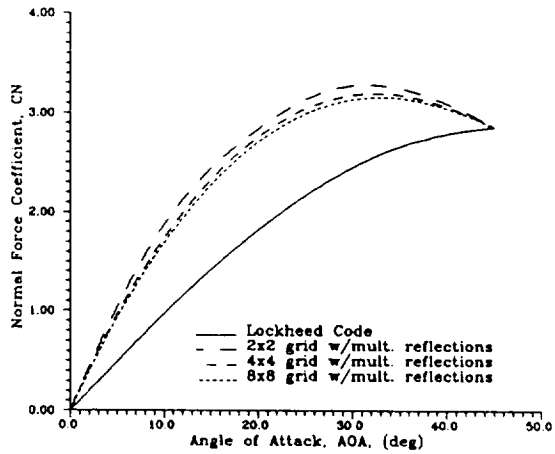

Fig. 6 Normal force coefficient for a 90° concave wedge with S_∞ = 7.5, T_w/T_∞ = 0.25, and $\alpha = \sigma_\eta = \sigma_\tau = 0$.

Because of the interrelatedness of the lift and drag coefficients to the axial and normal force coefficients, similar effects were expected for lift and drag. Fig. 7 shows the

variation in lift coefficient caused by the consideration of multiple reflections. The peak lift coefficient shifted from 25° AOA to 20° when multiple reflections are considered. The variation of results for the different grid sizes was more pronounced for the lift case than the axial or normal forces. The 2x2 results were nearly 10% higher than the 4x4 results for the 15° AOA case. The effects of grid size on drag coefficient were similar to the effects on the axial and normal forces. Figure 8 shows the large increase in drag coefficient possible when multiple reflections are considered. The 0° AOA case was, of course, the same as the axial force results for 0° AOA, but the same trend is apparent throughout the range of angles of attack.

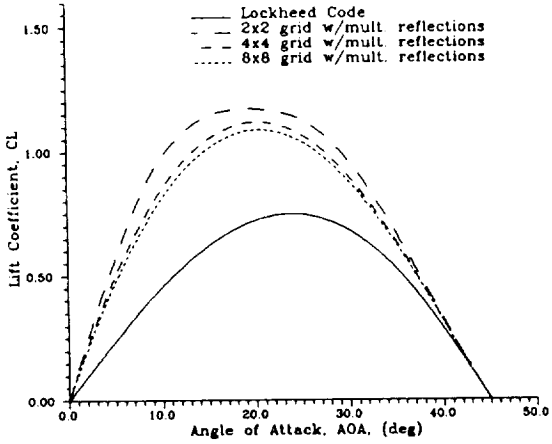

Fig. 7 Lift coefficient for a 90° concave wedge with $S_\infty = 7.5$, $T_w/T_\infty = 0.25$, and $\alpha = \sigma_\eta = \sigma_\tau = 0$.

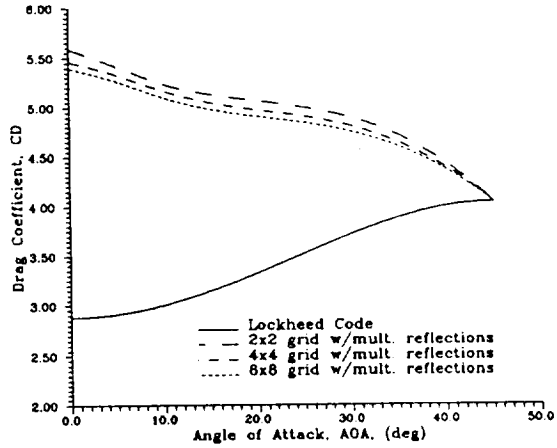

Fig. 8 Drag coefficient for a 90° concave wedge with $S_\infty = 7.5$, $T_w/T_\infty = 0.25$, and $\alpha = \sigma_\eta = \sigma_\tau = 0$.

As shown in Figure 9, the pitching moment did not have as drastic a change as lift and drag because of the reflected particles. Interestingly, the pitching moment coefficient increases over convex results for low angles of attack, but is lower for AOA greater than 10°. The 2x2 grid appeared to have difficulty handling the pitching moments. With only

two distinct moment arms for this calculation and all the forces applied at those two distances with a 2x2 grid, it is not really surprising the results weren't smooth.

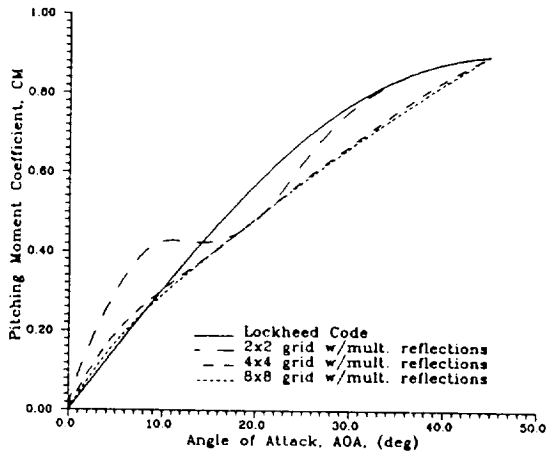

Fig. 9 Pitching moment coefficient for a 90° concave wedge with $S_\infty = 7.5$, $T_w/T_\infty = 0.25$, and $\alpha = \sigma_\eta = \sigma_\tau = 0$.

Results for $\alpha = 1.0$, $\sigma_\eta = 1.0$, $\sigma_\tau = 1.0$

The output values of force and moment coefficients for fully diffuse reflection are shown in Table 2. The axial and normal force coefficients, shown in Figs. 10 and 11,

Table 2 Force and moment coefficients for a 90° concave wedge with $S_\infty = 7.5$, $T_w/T_\infty = 0.25$, and $\alpha = \sigma_\eta = \sigma_\tau = 1.0$, 8x8 grid.

Results from Orbital Aerodynamics Code						Results with multiple reflect. effects					
AOA	C_A	C_N	C_L	C_D	C_M	AOA	C_A	C_N	C_L	C_D	C_M
0	2.9737	0	0	2.9737	0	0	2.9597	0	0	2.9597	0
5	2.9518	.256	-.0022	2.9629	.0804	5	2.9378	.2557	-.0013	2.949	.0804
10	2.8866	.5045	-.0044	2.9303	.1583	10	2.8729	.5037	-.0028	2.9167	.1585
15	2.7801	.7382	-.0065	2.8764	.2317	15	2.7667	.7368	-.0043	2.8632	.232
20	2.6355	.9501	-.0086	2.8015	.2982	20	2.6226	.9481	-.0061	2.7887	.2987
25	2.4571	1.1341	-.0106	2.7062	.3559	25	2.4449	1.1311	-.0081	2.6938	.3566
30	2.2504	1.2848	-.0125	2.5913	.4031	30	2.239	1.2806	-.0105	2.5793	.4041
35	2.0229	1.3993	-.014	2.4597	.4381	35	2.0126	1.3935	-.0129	2.4479	.4395
40	1.789	1.4828	-.0141	2.3236	.4573	40	1.7802	1.4749	-.0144	2.3118	.4592
45	1.6178	1.6178	0	2.2879	.4409	45	1.6106	1.6075	-.0022	2.2756	.4432

were essentially unchanged with the addition of the multiple reflection effects. The grid size did not affect the multiple reflection effects to a significant extent.

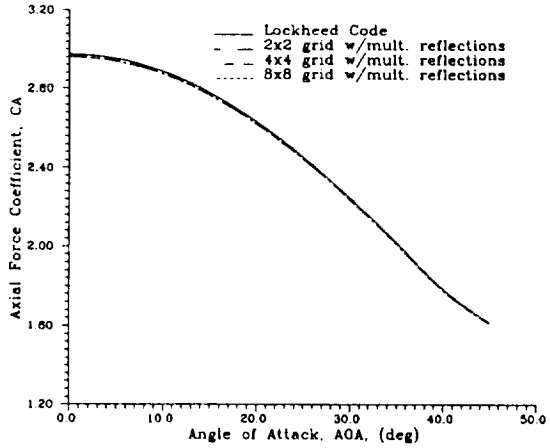

Fig. 10 Axial force coefficient for a 90° concave wedge with $S_\infty = 7.5$, $T_w/T_\infty = 0.25$, and $\alpha = \sigma_\eta = \sigma_\tau = 1$.

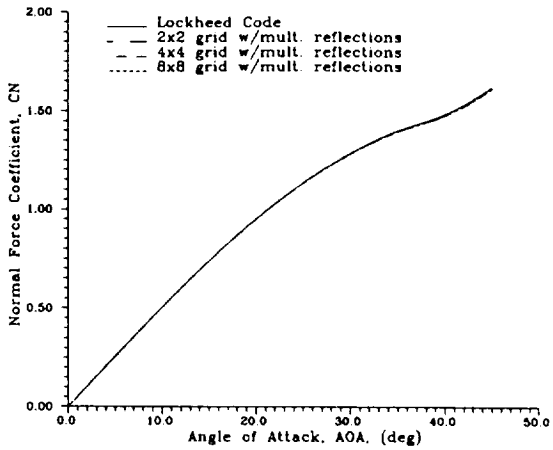

Fig. 11 Normal force coefficient for a 90° concave wedge with $S_\infty = 7.5$, $T_w/T_\infty = 0.25$, and $\alpha = \sigma_\eta = \sigma_\tau = 1$.

The lift coefficient, shown in Fig. 12, had a noticeable percentage change (over 30%) due to multiple reflections in the lower angles of attack. The magnitude of the lift coefficient for this case only had a maximum absolute value of 0.0144, and the maximum change was 0.0025. This would be a very small force indeed. The grid spacing had only a minute effect.

There was only a small reduction in the drag coefficient, as seen in Fig. 13. The reduction was only about 0.5%. The multiple reflection results for the different grid spacings were all right at the same values.

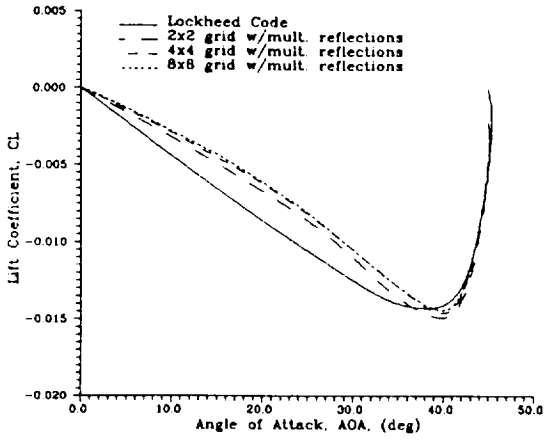

Fig. 12 Lift coefficient for a 90° concave wedge with $S_\infty = 7.5$, $T_w/T_\infty = 0.25$, and $\alpha = \sigma_\eta = \sigma_\tau = 1$.

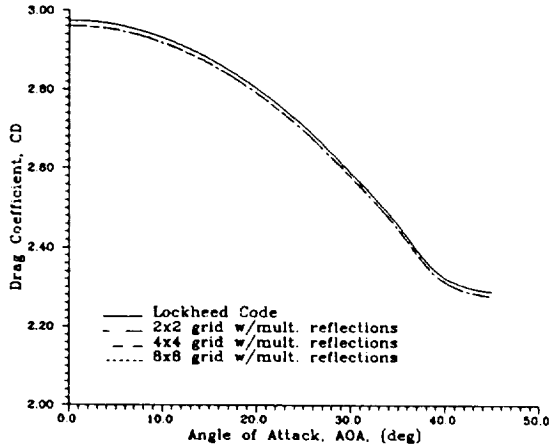

Fig. 13 Drag coefficient for a 90° concave wedge with $S_\infty = 7.5$, $T_w/T_\infty = 0.25$, and $\alpha = \sigma_\eta = \sigma_\tau = 1$.

Figure 14 shows the nearly identical plots of pitching moment for the convex and concave cases. The magnitude of the difference is a maximum of 0.001.

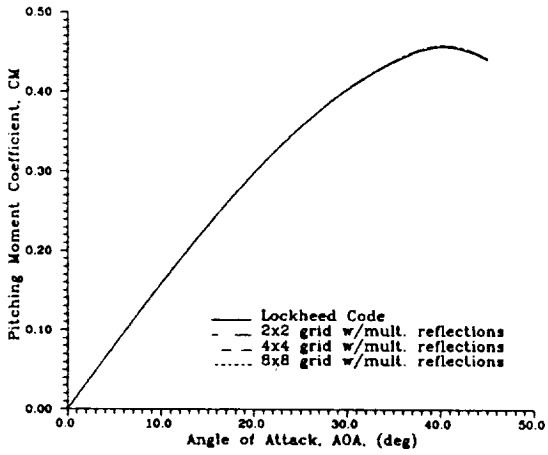

Fig. 14 Pitching moment coefficient for a 90° concave wedge with $S_\infty = 7.5$, $T_w/T_\infty = 0.25$, and $\alpha = \sigma_\eta = \sigma_\tau = 1$.

Results for $\alpha = 0.9$, $\sigma_\eta = 1.0$, $\sigma_\tau = 1.0$

Values for the force and moment coefficients for full momentum accommodation and energy accommodation of 0.9 can be found in Table 3. Figures 15 and 16 display the axial and normal force coefficients for this case. The alteration of the energy accommodation resulted in virtually no change from the fully diffuse case.

Table 3 Force and moment coefficients for a 90° concave wedge with $S_\infty = 7.5$, $T_w/T_\infty = 0.25$, and $\alpha = 0.9$, $\sigma_\eta = \sigma_\tau = 1.0$, 8x8 grid.

Results from Orbital Aerodynamics Code						Results with multiple reflect. effects					
AOA	C_A	C_N	C_L	C_D	C_M	AOA	C_A	C_N	C_L	C_D	C_M
0	2.9737	0	0	2.9737	0	0	2.9646	0	0	2.9646	0
5	2.9518	.256	-.0022	2.9629	.0804	5	2.9427	.256	-.0015	2.9538	.0804
10	2.8866	.5045	-.0044	2.9303	.1583	10	2.8776	.5044	-.0029	2.9214	.1584
15	2.7801	.7382	-.0065	2.8764	.2317	15	2.7712	.738	-.0044	2.8677	.2317
20	2.6355	.9501	-.0086	2.8015	.2982	20	2.6267	.9497	-.006	2.7931	.2983
25	2.4571	1.1341	-.0106	2.7062	.3559	25	2.4486	1.1333	-.0077	2.6981	.3561
30	2.2504	1.2848	-.0125	2.5913	.4031	30	2.2423	1.2834	-.0097	2.5836	.4035
35	2.0229	1.3993	-.014	2.4597	.4381	35	2.0155	1.3968	-.0119	2.4522	.4386
40	1.789	1.4828	-.0141	2.3236	.4573	40	1.7829	1.4786	-.0133	2.3162	.4583
45	1.6178	1.6178	0	2.2879	.4409	45	1.6133	1.6113	-.0014	2.2801	.4423

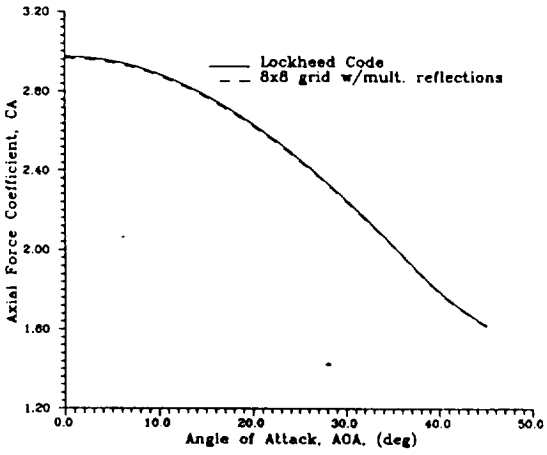

Fig. 15 Axial force coefficient for a 90° concave wedge with $S_\infty = 7.5$, $T_w/T_\infty = 0.25$, and $\alpha = 0.9$, $\sigma_\eta = \sigma_\tau = 1.0$.

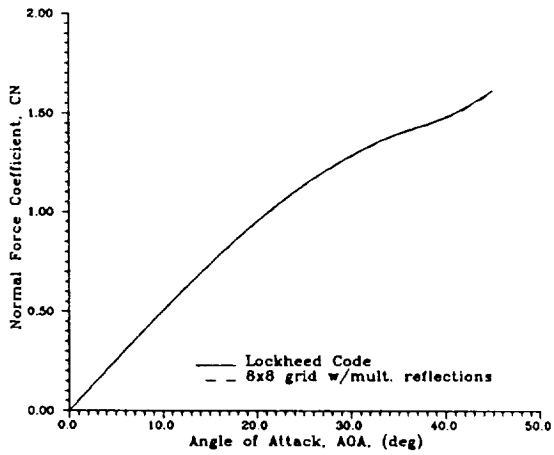

Fig. 16 Normal force coefficient for a 90° concave wedge with $S_\infty = 7.5$, $T_w/T_\infty = 0.25$, and $\alpha = 0.9$, $\sigma_\eta = \sigma_\tau = 1.0$.

Figure 17 shows the lift coefficient on the concave and convex wedges for angles

of attack from 0° to 45°. The results with multiple reflections were slightly less than for the fully diffuse case. The concave results were up to 30% less (in absolute value) than the convex results. For AOA from 40° to 45°, the concave lift coefficient was still less than the convex case, where the fully diffuse lift coefficient was slightly greater than the convex case. The magnitude of the change and the actual value of lift coefficients were very small, as in the diffuse case. The drag coefficient results, shown in Fig 18, were not changed significantly from the diffuse case of Fig. 13 for either convex or concave. Changes were less than 0.5%.

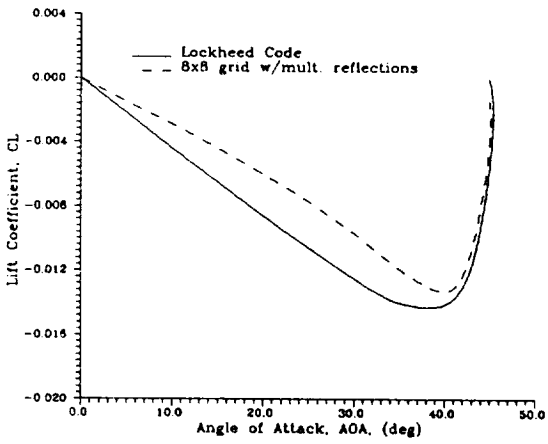

Fig. 17 Lift force coefficient for a 90° concave wedge with $S_\infty = 7.5$, $T_w/T_\infty = 0.25$, and $\alpha = 0.9$, $\sigma_\eta = \sigma_\tau = 1.0$.

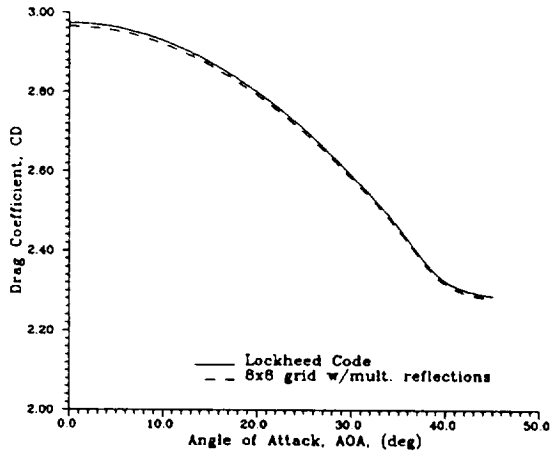

Fig. 18 Drag force coefficient for a 90° concave wedge with $S_\infty = 7.5$, $T_w/T_\infty = 0.25$, and $\alpha = 0.9$, $\sigma_\eta = \sigma_\tau = 1.0$.

Figure 19 shows the pitching moment coefficient results for the wedge. The concave and convex results were indistinguishable from each other, and from the diffuse case.

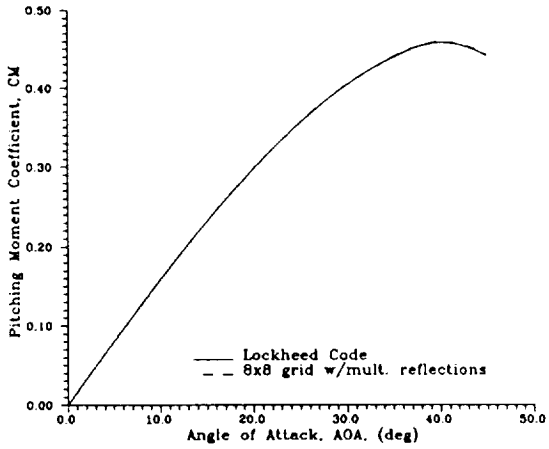

Fig. 19 Pitching moment coefficient for a 90° concave wedge with $S_\infty = 7.5$, $T_w/T_\infty = 0.25$, and $\alpha = 0.9$, $\sigma_\eta = \sigma_\tau = 1.0$.

Results for $\alpha = 0.9$, $\sigma_\eta = 0.9$, $\sigma_\tau = 0.9$

The results for the case with all accommodation equal to 0.9 are contained in Table 4. As shown in Fig. 20, the convex axial force coefficient results were nearly the same as the diffuse case. However, there was a more significant change in the concave results for this accommodation case. The axial force at 0° angle of attack was reduced from 2.96 to 2.88, a 2.7% change. The normal force also changed with the addition of multiple reflections. Figure 21 shows, for instance, the increase in normal force coefficient from 1.23 to 1.33 for 25° AOA. This is about a 7.7% increase in the coefficient.

Figure 22 shows the change in lift coefficient due to the consideration of multiple reflections. When all accommodation values were 0.9, there was a positive lift force, unlike the diffuse case. The lift was still small in magnitude, 0.065 at 25° AOA for the convex case. The increase in lift coefficient due to multiple reflections was 0.11 at 25° AOA, so the percentage increases were very large. At 40° AOA, the multiple reflection

lift coefficient was 251% greater than the convex result.

Table 4 Force and moment coefficients for a 90° concave wedge with S_∞ = 7.5, T_w/T_∞ = 0.25, and $\alpha = \sigma_\eta = \sigma_\tau = 0.9$, 8x8 grid.

Results from Orbital Aerodynamics Code						Results with multiple reflect. effects					
AOA	C_A	C_N	C_L	C_D	C_M	AOA	C_A	C_N	C_L	C_D	C_M
0	2.9644	0	0	2.9644	0	0	2.8846	0	0	2.8846	0
5	2.9447	.2796	.0219	2.9578	.0877	5	2.8658	.3077	.0567	2.8817	.0852
10	2.886	.5509	.0414	2.9378	.1729	10	2.8095	.6048	.1077	2.8718	.1681
15	2.7901	.8059	.0563	2.9037	.2529	15	2.7176	.8812	.1478	2.853	.2463
20	2.66	1.037	.0647	2.8543	.3254	20	2.5933	1.1269	.1719	2.8223	.3175
25	2.4995	1.2375	.0652	2.7883	.3883	25	2.4406	1.3331	.1768	2.7753	.3798
30	2.3134	1.4014	.057	2.7042	.4397	30	2.2652	1.4896	.1575	2.7066	.4319
35	2.1086	1.5254	.0401	2.6022	.4778	35	2.0734	1.5933	.1159	2.6123	.472
40	1.898	1.6135	.016	2.491	.4991	40	1.8778	1.6491	.0562	2.4985	.4966
45	1.7416	1.7416	0	2.4629	.4864	45	1.7377	1.7357	-.0014	2.456	.4876

The drag coefficient for the wedge in free molecule flow is shown in Fig. 23. The convex results were similar to the diffuse case, but the concave results were reduced by 0.08 at 0° AOA (2.7% change).

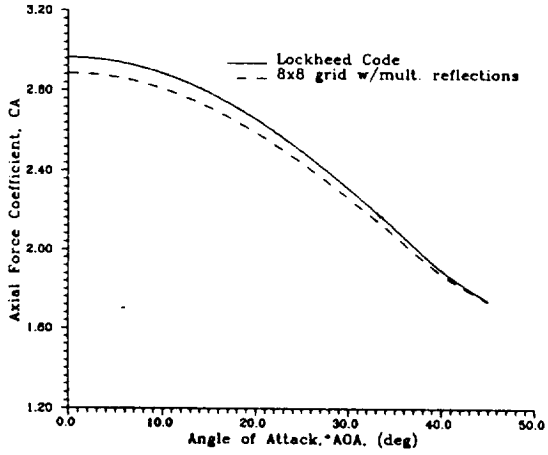

Fig. 20 Axial force coefficient for a 90° concave wedge with S_∞ = 7.5, T_w/T_∞ = 0.25, and $\alpha = \sigma_\eta = \sigma_\tau = 0.9$.

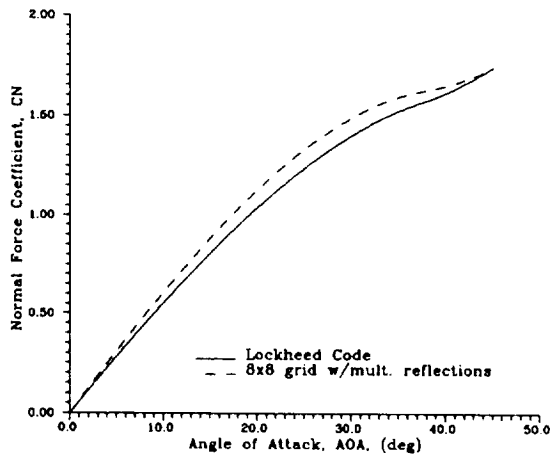

Fig. 21 Normal force coefficient for a 90° concave wedge with S_∞ = 7.5, T_w/T_∞ = 0.25, and $\alpha = \sigma_\eta = \sigma_\tau = 0.9$.

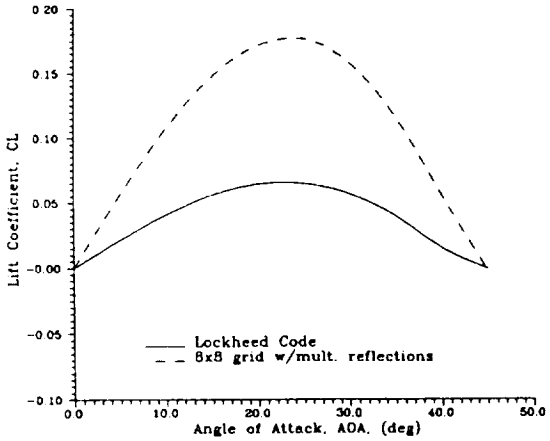

Fig. 22 Lift force coefficient for a 90° concave wedge with $S_\infty = 7.5$, $T_w/T_\infty = 0.25$, and $\alpha = \sigma_\eta = \sigma_\tau = 0.9$.

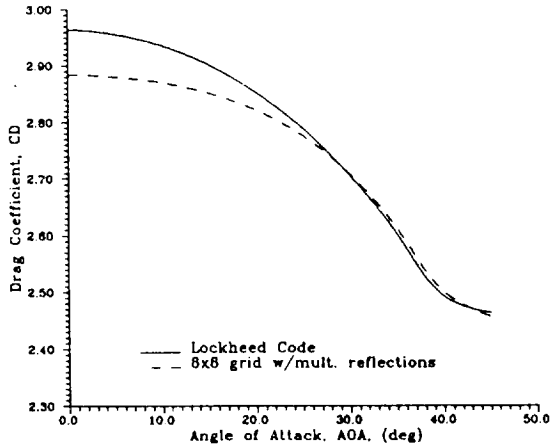

Fig. 23 Drag force coefficient for a 90° concave wedge with $S_\infty = 7.5$, $T_w/T_\infty = 0.25$, and $\alpha = \sigma_\eta = \sigma_\tau = 0.9$.

Figure 24 shows the concave and convex pitching moment coefficients. The concave results were just distinguishable from the convex results for angles of attack from 10° to 40°. There was a reduction of up to 0.008 (about 2%) in that range.

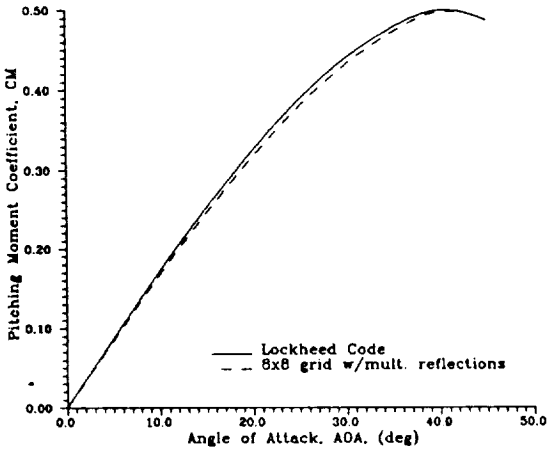

Fig. 24 Pitching moment coefficient for a 90° concave wedge with $S_\infty = 7.5$, $T_w/T_\infty = 0.25$, and $\alpha = \sigma_\eta = \sigma_\tau = 0.9$.

Results for $\alpha = 0.7$, $\sigma_\eta = 0.6$, $\sigma_\tau = 0.6$

For the test case with energy accommodation of 0.7 and both tangential and normal momentum accommodation of 0.6 the calculated force and moment coefficients for convex and concave wedges are displayed in Table 5. Figure 25 shows the results for the axial force coefficient. The addition of reflected particles increased the axial force from 7% to 10% over most of the range of angles of attack, with the greatest physical change, 0.25 (8.9%), at 15° AOA. The greatest change in normal force coefficient was 0.53 (41% increase) at 20° AOA, as shown in Fig. 26. The normal force coefficient with multiple reflections has a more pronounced maximum point at 35°, while the convex coefficient has no internal maximum in the range of angles of attack from 0° to 45°.

Table 5 Force and moment coefficients for a 90° concave wedge with $S_\infty = 7.5$, $T_w/T_\infty = 0.25$, and $\alpha = 0.7$, $\sigma_\eta = \sigma_\tau = 0.6$, 8x8 grid.

Results from Orbital Aerodynamics Code						Results with multiple reflect. effects					
AOA	C_A	C_N	C_L	C_D	C_M	AOA	C_A	C_N	C_L	C_D	C_M
0	2.9365	0	0	2.9365	0	0	3.1581	0	0	3.1581	0
5	2.9233	.3502	.0941	2.9427	.1099	5	3.1509	.5686	.2918	3.1885	.1359
10	2.8842	.6899	.1786	2.9602	.2165	10	3.1261	1.0839	.5246	3.2668	.2636
15	2.8203	1.009	.2446	2.9853	.3166	15	3.0716	1.5085	.6621	3.3574	.3747
20	2.7336	1.2978	.2846	3.0126	.4073	20	2.9799	1.8272	.6978	3.4252	.466
25	2.6265	1.5477	.2927	3.0345	.4857	25	2.8526	2.0472	.6498	3.4505	.5372
30	2.5025	1.7513	.2655	3.0429	.5496	30	2.6907	2.1686	.5327	3.4145	.59
35	2.3659	1.9035	.2023	3.0298	.5968	35	2.5015	2.202	.369	3.3121	.6241
40	2.2248	2.0055	.1062	2.9934	.6246	40	2.2961	2.1608	.1794	3.1478	.6382
45	2.1129	2.1129	0	2.988	.623	45	2.1116	2.1103	-.0009	2.9853	.6233

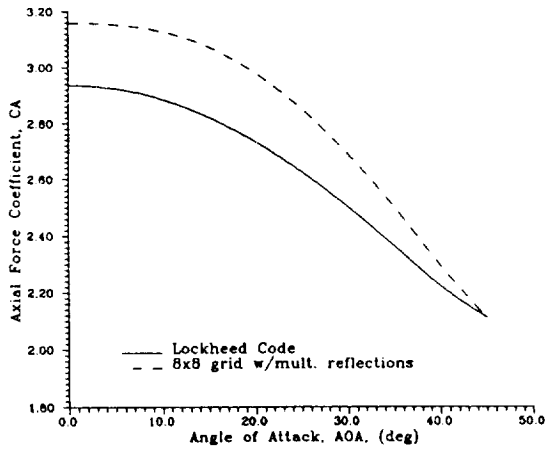

Fig. 25 Axial force coefficient for a 90° concave wedge with $S_\infty = 7.5$, $T_w/T_\infty = 0.25$, and $\alpha = 0.7$, $\sigma_\eta = \sigma_\tau = 0.6$.

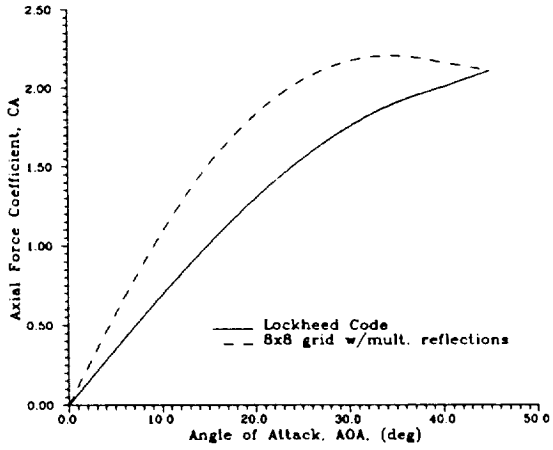

Fig. 26 Normal force coefficient for a 90° concave wedge with $S_\infty = 7.5$, $T_w/T_\infty = 0.25$, and $\alpha = 0.7$, $\sigma_\eta = \sigma_\tau = 0.6$.

Figure 27 shows the lift coefficient for the test configuration for angles of attack from 0° to 45°. The increases in the lift coefficient with the addition of multiple reflections were in the range of 0.3 to 0.4 over most of the angles of attack. The changes were large in terms of percentage (100% to 200%) because of the low values of lift coefficient for the convex case. Figure 28 shows the changes in the drag coefficient due to the addition of multiple reflections. The magnitude of the changes was similar to the changes in lift coefficient, but because of the large values of convex wedge drag coefficient, the percentage change was less than 14%. The character of the drag coefficient was somewhat different for this accommodation case. The drag coefficient for the more diffuse accommodation cases was a maximum at 0° AOA and decreased regularly for higher angles of attack. For this case, the drag coefficient increased for angles of attack greater than 0° up to 30° and then decreased slightly. The coefficient with concave effects followed this pattern, but had a much greater decrease from 30° to 45° AOA.

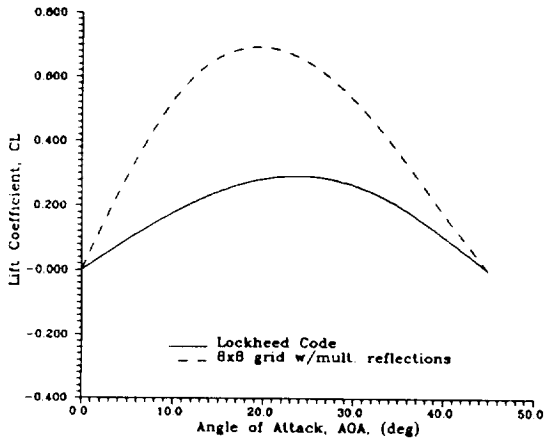

Fig. 27 Lift force coefficient for a 90° concave wedge with $S_\infty = 7.5$, $T_w/T_\infty = 0.25$, and $\alpha = 0.7$, $\sigma_\eta = \sigma_\tau = 0.6$.

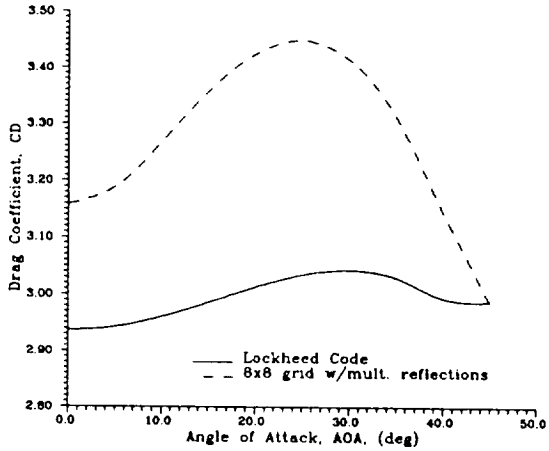

Fig. 28 Drag force coefficient for a 90° concave wedge with $S_\infty = 7.5$, $T_w/T_\infty = 0.25$, and $\alpha = 0.7$, $\sigma_\eta = \sigma_\tau = 0.6$.

The increase in pitching moment due to the consideration of concave surface effects is evident in Fig. 29. Changes found in the pitching moment were fairly small, on the order of 0.05, with the largest absolute increase at 20° AOA. The increase at 20° was 0.059 or 14.4%.

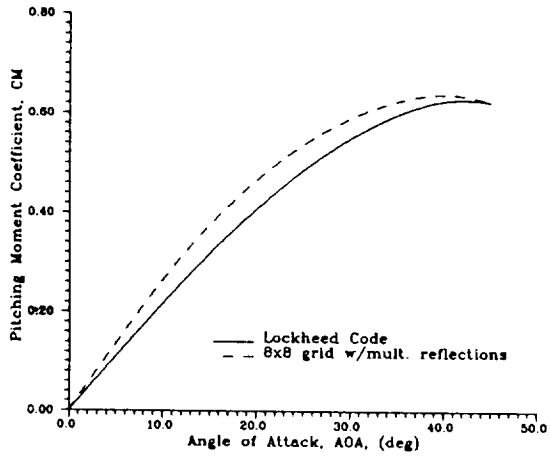

Fig. 29 Pitching moment coefficient for a 90° concave wedge with $S_\infty = 7.5$, $T_w/T_\infty = 0.25$, and $\alpha = 0.7$, $\sigma_\eta = \sigma_\tau = 0.6$.

Results for $\alpha = 0.5$, $\sigma_\eta = 0.4$, $\sigma_\tau = 0.4$

The case with energy accommodation of 0.5 and momentum accommodation of 0.4 followed the same trends as the cases discussed above. The results are presented in Table 6. The force coefficient in the axial direction for angles of attack from 0° to 45° is shown in Fig. 30. The increase in axial force coefficient at 0° was 0.80, or about 27.7%. The 27.7% increase was nearly four times the increase found in the $\alpha = 0.7$ case. The convex and concave results converged at 45° AOA, as before. Figure 31 shows the coefficient for the normal force on the wedge. The maximum change in normal force was a 0.69 increase at 20°. The increases at lower angle of attack were higher percentage changes, up to 83%, but 0.69 was the greatest physical change.

Table 6 Force and moment coefficients for a 90° concave wedge with $S_\infty = 7.5$, $T_w/T_\infty = 0.25$, and $\alpha = 0.5$, $\sigma_\eta = \sigma_\tau = 0.4$, 8x8 grid.

Results from Orbital Aerodynamics Code						Results with multiple reflect. effects					
AOA	C_A	C_N	C_L	C_D	C_M	AOA	C_A	C_N	C_L	C_D	C_M
0	2.9179	0	0	2.9179	0	0	3.7256	0	0	3.7256	0
5	2.9091	.3973	.1422	2.9326	.1247	5	3.7078	.7282	.4023	3.7571	.1828
10	2.883	.7826	.2701	2.9751	.2456	10	3.6549	1.3426	.6875	3.8325	.3377
15	2.8404	1.1444	.3702	3.0398	.3591	15	3.5544	1.8141	.8323	3.9028	.4564
20	2.7826	1.4716	.4312	3.1181	.4618	20	3.4141	2.1573	.8596	3.946	.546
25	2.7112	1.7545	.4443	3.1987	.5506	25	3.242	2.3856	.7919	3.9465	.6134
30	2.6285	1.9846	.4044	3.2687	.6228	30	3.0433	2.506	.6486	3.8885	.6635
35	2.5374	2.1557	.3104	3.3149	.6761	35	2.8233	2.5267	.4503	3.762	.6986
40	2.4427	2.2668	.1664	3.3283	.7082	40	2.5893	2.4596	.2198	3.5645	.7176
45	2.3604	2.3604	0	3.3381	.714	45	2.36	2.3589	-.0007	3.3368	.7141

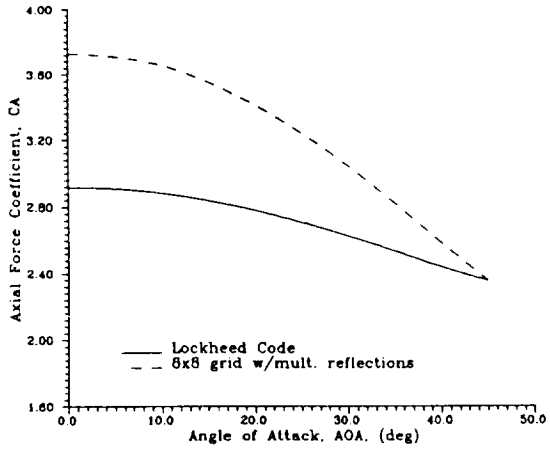

Fig. 30 Axial force coefficient for a 90° concave wedge with $S_\infty = 7.5$, $T_w/T_\infty = 0.25$, and $\alpha = 0.5$, $\sigma_\eta = \sigma_\tau = 0.4$.

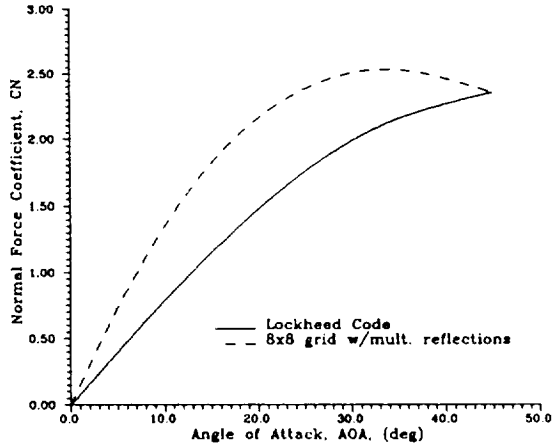

Fig. 31 Normal force coefficient for a 90° concave wedge with $S_\infty = 7.5$, $T_w/T_\infty = 0.25$, and $\alpha = 0.5$, $\sigma_\eta = \sigma_\tau = 0.4$.

The changes in the coefficient of lift are shown in Fig. 32. The addition of multiple reflections acted to increase the lift coefficient, and move the point of maximum lift from 25° AOA without multiple reflections to around 20° with multiple reflections. The coefficient was increased a maximum of 0.46 at 15° AOA (124%). There was a 183% increase in lift at 5° AOA.

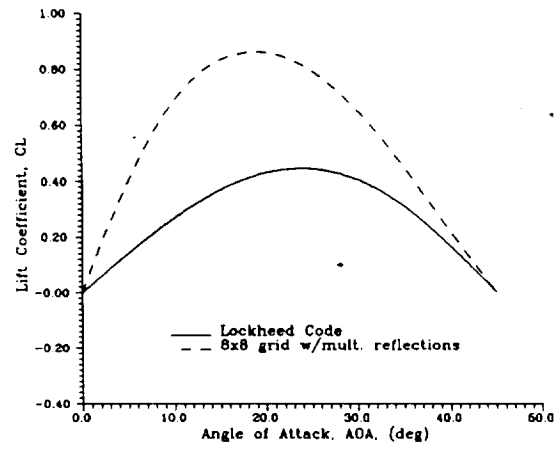

Fig. 32 Lift force coefficient for a 90° concave wedge with $S_\infty = 7.5$, $T_w/T_\infty = 0.25$, and $\alpha = 0.5$, $\sigma_\eta = \sigma_\tau = 0.4$.

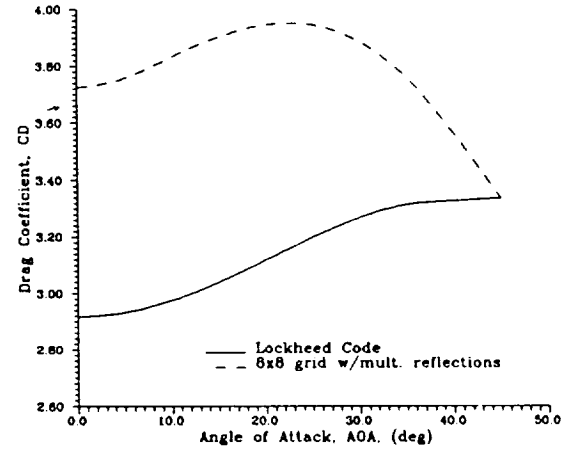

Fig. 33 Drag force coefficient for a 90° concave wedge with $S_\infty = 7.5$, $T_w/T_\infty = 0.25$, and $\alpha = 0.5$, $\sigma_\eta = \sigma_\tau = 0.4$.

The drag force and pitching moment coefficient results are shown in Figs. 33 and 34. The point of maximum increases in drag and pitching moment were at 15° AOA. The drag coefficient increased a maximum of 0.863 (28%) and the moment coefficient increased a maximum of 0.097, or 27%, due to the concave effects.

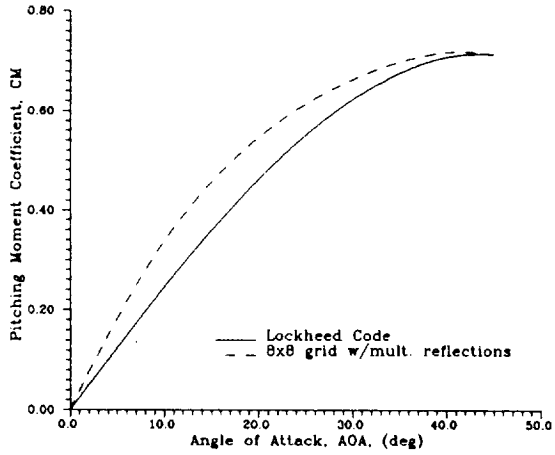

Fig. 34 Pitching moment coefficient for a 90° concave wedge with $S_\infty = 7.5$, $T_w/T_\infty = 0.25$, and $\alpha = 0.5$, $\sigma_\eta = \sigma_\tau = 0.4$.

Results for $\alpha = 0.3$, $\sigma_\eta = 0.2$, $\sigma_\tau = 0.2$

Data from calculations of force and moment coefficients for energy accommodation of 0.3 and momentum accommodation of 0.2 is presented in Table 7. The results for axial force and normal force coefficients are shown in Figs. 35 and 36. The axial force coefficient increased by 1.72 with the addition of multiple reflections for an AOA of 0°. That was a 59% increase.

The normal force coefficient increased about 48% to 2.44 at a 20° angle of attack. There was significant change in the normal coefficient over the whole range of tested angles of attack.

Table 7 Force and moment coefficients for a 90° concave wedge with S_∞ = 7.5, T_w/T_∞ = 0.25, and α = 0.3, $\sigma_\eta = \sigma_\tau$ = 0.2, 8x8 grid.

Results from Orbital Aerodynamics Code						Results with multiple reflect. effects					
AOA	C_A	C_N	C_L	C_D	C_M	AOA	C_A	C_N	C_L	C_D	C_M
0	2.8993	0	0	2.8993	0	0	4.6208	0	0	4.6208	0
5	2.8949	.4444	.1904	2.9226	.1395	5	4.5289	.8551	.4571	4.5862	.1919
10	2.8818	.8753	.3616	2.99	.2747	10	4.3441	1.5405	.7628	4.5456	.3313
15	2.8605	1.2798	.4958	3.0943	.4016	15	4.1183	2.06	.9239	4.5112	.4321
20	2.8316	1.6455	.5778	3.2236	.5164	20	3.879	2.438	.9642	4.4789	.5143
25	2.7959	1.9613	.596	3.3629	.6155	25	3.6354	2.689	.9007	4.4312	.5883
30	2.7546	2.2179	.5434	3.4945	.696	30	3.3882	2.8203	.7484	4.3444	.6566
35	2.7089	2.4078	.4186	3.6	.7554	35	3.1355	2.8377	.526	4.1961	.718
40	2.6605	2.5282	.2266	3.6632	.7918	40	2.8763	2.7521	.2593	3.9724	.7688
45	2.6079	2.6079	0	3.6882	.8051	45	2.608	2.6071	-.0006	3.6876	.805

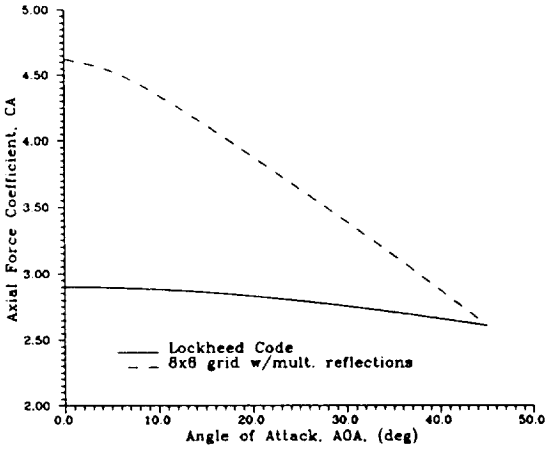

Fig. 35 Axial force coefficient for a 90° concave wedge with S_∞ = 7.5, T_w/T_∞ = 0.25, and α = 0.3, $\sigma_\eta = \sigma_\tau$ = 0.2.

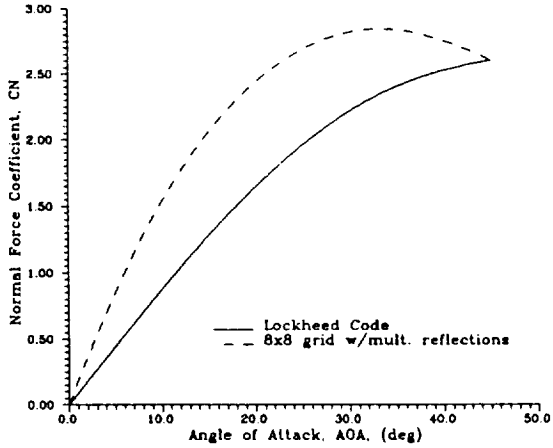

Fig. 36 Normal force coefficient for a 90° concave wedge with S_∞ = 7.5, T_w/T_∞ = 0.25, and α = 0.3, $\sigma_\eta = \sigma_\tau$ = 0.2.

The results for the coefficient of lift are shown in Fig. 37. The lift calculated by the convex method was greater than that of the more diffuse accommodation cases, but the amount of increase due to multiple reflections is not much different. The coefficient at 15° AOA increased 0.43, but the percentage change for this accommodation case was only 86%.

Figure 38 shows the drag coefficient of the wedge over angles of attack from 0° to 45°. The maximum increase due to multiple reflections was at 0° AOA, where a change

of 1.72 (59%) was present. The shape of the lift and drag plots for this accommodation was comparable to the specular case.

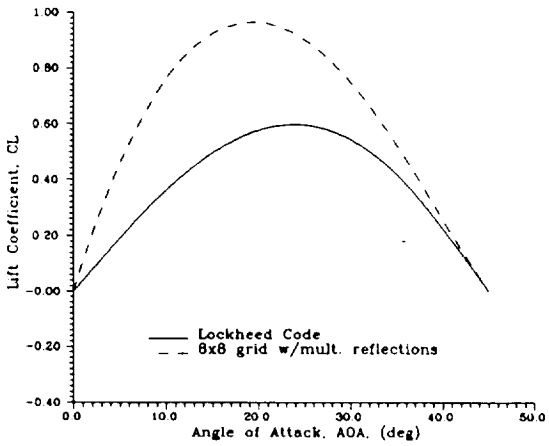

Fig. 37 Lift force coefficient for a 90° concave wedge with $S_\infty = 7.5$, $T_w/T_\infty = 0.25$, and $\alpha = 0.3$, $\sigma_\eta = \sigma_\tau = 0.2$.

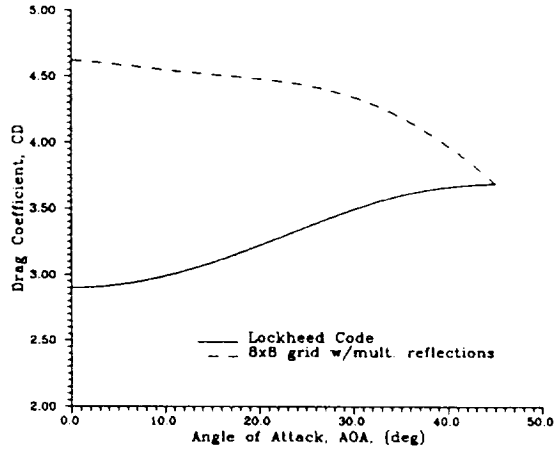

Fig. 38 Drag force coefficient for a 90° concave wedge with $S_\infty = 7.5$, $T_w/T_\infty = 0.25$, and $\alpha = 0.3$, $\sigma_\eta = \sigma_\tau = 0.2$.

The results for the pitching moment coefficient for the convex and concave wedge are shown in Fig. 39. Multiple reflections acted to increase the pitching moment for angles of attack from 0° to 20°. From 20° up to 45°, the pitching moment decreased compared to the convex case. The increase at 10° was 0.056 (20%), and the decrease at 30° was 0.039 (5.7%).

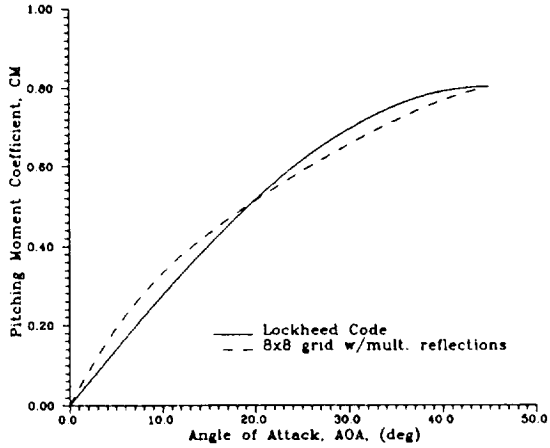

Fig. 39 Pitching moment coefficient for a 90° concave wedge with $S_\infty = 7.5$, $T_w/T_\infty = 0.25$, and $\alpha = 0.3$, $\sigma_\eta = \sigma_\tau = 0.2$.

Results for $\alpha = 0.1$, $\sigma_\eta = 0.1$, $\sigma_\tau = 0.1$

Table 8 contains the output data from the calculations for the wedge in free molecule flow with surface accommodation of $\alpha = \sigma_\eta = \sigma_\tau = 0.1$. The axial force coefficient is shown in Fig. 40 and the normal force coefficient results are shown in Fig. 41. The axial force coefficient was greatly increased by the addition of multiple reflections with an increase of 1.92 at 0° AOA. The normal force also had some large increases from 10° to 30° AOA, with the largest increase, 0.82 (47%) at 20° AOA.

Table 8 Force and moment coefficients for a 90° concave wedge with S_∞ = 7.5, T_w/T_∞ = 0.25, and $\alpha = \sigma_\eta = \sigma_\tau = 0.1$, 8x8 grid.

Results from Orbital Aerodynamics Code						Results with multiple reflect. effects					
AOA	C_A	C_N	C_L	C_D	C_M	AOA	C_A	C_N	C_L	C_D	C_M
0	2.8899	0	0	2.8899	0	0	4.8157	0	0	4.8157	0
5	2.8877	.4679	.2145	2.9175	.1469	5	4.7108	.9041	.4901	4.7717	.2142
10	2.8812	.9217	.4074	2.9975	.2892	10	4.5042	1.62	.8132	4.7171	.3621
15	2.8706	1.3475	.5586	3.1215	.4229	15	4.258	2.161	.9853	4.6722	.466
20	2.8561	1.7324	.651	3.2764	.5437	20	4.0032	2.5552	1.0319	4.6357	.5508
25	2.8383	2.0647	.6718	3.445	.648	25	3.751	2.8186	.9693	4.5907	.6275
30	2.8176	2.3345	.6129	3.6074	.7326	30	3.5015	2.9579	.8109	4.5114	.6981
35	2.7947	2.5338	.4726	3.7426	.7951	35	3.2519	2.9783	.5745	4.3721	.7611
40	2.7695	2.6589	.2566	3.8306	.8336	40	2.9994	2.8902	.2861	4.1554	.8124
45	2.7317	2.7317	0	3.8632	.8506	45	2.7319	2.7312	-.0005	3.863	.8505

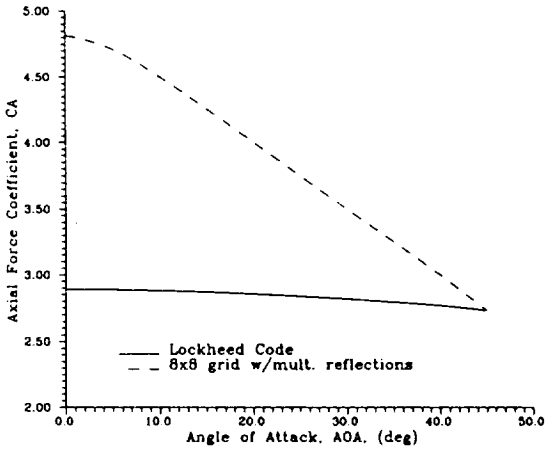

Fig. 40 Axial force coefficient for a 90° concave wedge with S_∞ = 7.5, T_w/T_∞ = 0.25, and $\alpha = \sigma_\eta = \sigma_\tau = 0.1$.

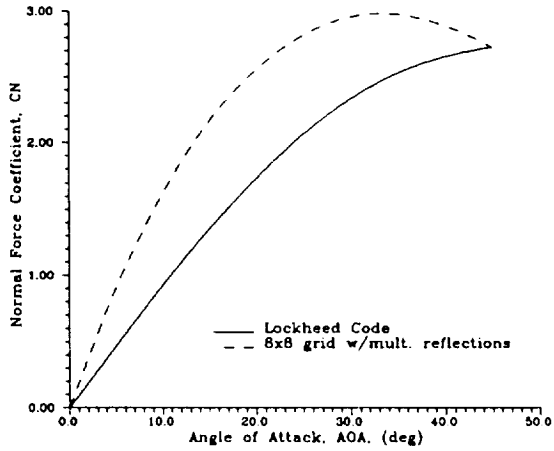

Fig. 41 Normal force coefficient for a 90° concave wedge with S_∞ = 7.5, T_w/T_∞ = 0.25, and $\alpha = \sigma_\eta = \sigma_\tau = 0.1$.

Figure 42 shows the lift coefficient for the wedge at this accommodation case. The largest increase was 0.43 at 15°, but the increase in lift coefficient between 0° and 15° was near 100%. The angles of attack greater than 30° did not show nearly as great an increase. The angle of attack of maximum lift coefficient also shifted to lower AOA for the concave case.

The drag coefficient is shown in Fig. 43. The increase in drag was dramatic, and nearly as great as for specular reflection; the drag coefficient at 0° changed from 2.89 to

4.82 (67%). Also significant was the fact that with increasing angle of attack, the concave drag coefficient always decreased while the convex drag coefficient always increased.

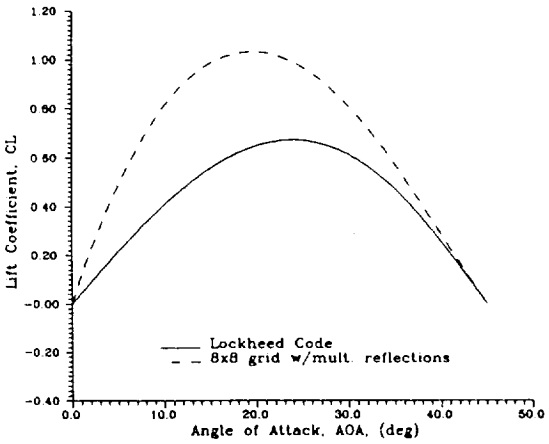

Fig. 42 Lift force coefficient for a 90° concave wedge with $S_\infty = 7.5$, $T_w/T_\infty = 0.25$, and $\alpha = \sigma_\eta = \sigma_\tau = 0.1$.

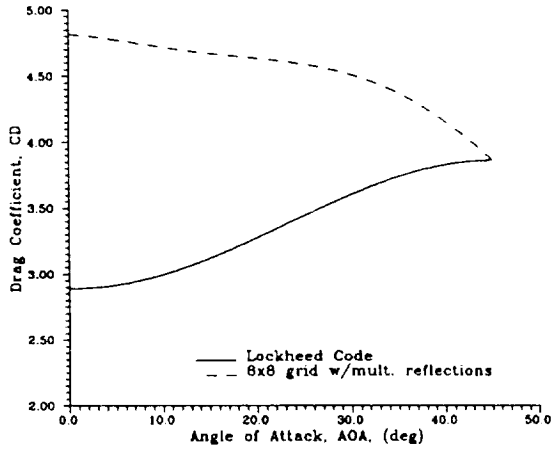

Fig. 43 Drag force coefficient for a 90° concave wedge with $S_\infty = 7.5$, $T_w/T_\infty = 0.25$, and $\alpha = \sigma_\eta = \sigma_\tau = 0.1$.

The pitching moment is shown in Fig. 44. Only the accommodation cases with $\alpha = 0.5$ and $\sigma_\eta = \sigma_\tau = 0.4$ and the fully specular case had larger absolute value changes in the pitching moment. The intermediate accommodation case only had an increase in the pitching moment, but this case was like the specular case that had an increase at low angle of attack and a decrease at higher angles of attack. The largest increase was 0.073 at 10° AOA, or about 25%.

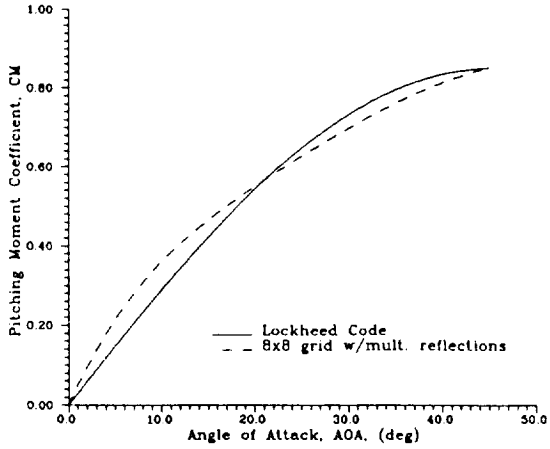

Fig. 44 Pitching moment coefficient for a 90° concave wedge with $S_\infty = 7.5$, $T_w/T_\infty = 0.25$, and $\alpha = \sigma_\eta = \sigma_\tau = 0.1$.

Discussion

There were several points that deserve to be discussed further. A major point to note is the difference between the cases where a body is considered to be convex (no multiply reflected particles) with full diffuse accommodation and the case calculated here with a concave body (including multiple reflections) and all accommodation coefficients set equal to 0.9. It is common practice for diffuse reflection without multiple reflection of molecules to be used to model vehicles in free molecule flow. However, from most available data, 0.9 is probably closer to an actual value of surface accommodation for many engineering surfaces. As shown in Figs. 22 and 23, there could be a significant change in forces produced for these models. Also, it is not always intuitively obvious whether the addition of multiple reflections will increase or decrease a force or moment applied to a complex configuration.

The range of angles of attack was chosen to be from 0° to 45°. It was obviously

not necessary to evaluate angles less than 0° because of the symmetry of the test configuration. At 45°, the #I plate is perpendicular to the flow and plate #II is edge-on to the flow. Because a plate that is edge on to the flow can have momentum transferred to it by the flow, it was necessary to include subshape #III on the underside of plate #II to balance the normal force on plate II by diffusely reflecting particles. Beyond 45°, the bottom subshapes, II and III, would shield subshape I from some incident flow. Because of the right angle between the plates, specular flow from plate I would never hit subshape II and the results should be the same as the convex case. At the other extreme of diffuse reflection, particles reflected from subshape I would not likely have a measurable effect on subshape II since we have seen the small contribution that diffusely reflected particles have on force and moment coefficients. To actually include these cases in the study would require a new method of checking for shielding of subshapes from the reflected flow from other elements.

CONCLUSION

Force and moment coefficients for a 90° wedge, in free molecule flow with speed ratio 7.5, with and without considering multiply reflected molecules were reported. The wedge was composed of two square flat plates of unit area joined at one edge with right included angle. The traditionally limiting cases of specular and diffuse reflection showed that multiple reflection of molecules could have a very significant effect for specular reflection, but almost no measurable effect in the case of diffuse reflections. In addition to the limiting cases, several cases of intermediate accommodation were also calculated. The magnitude of effect of the multiple reflections for the intermediate accommodation cases was more significant for accommodation values near the specular range. However, even for the nearly diffuse case with $\alpha = \sigma_\eta = \sigma_\tau = 0.9$, modeling a wedge as concave resulted in significant changes from the convex results.

For the case of specular reflection, the axial force and drag coefficients increased by an amount in excess of 2.51 when the test configuration was at an angle of attack (AOA) of 0°. This was just over an 87% increase over the coefficient value of the results without multiple reflections. The effect of multiple reflection diminished with increasing angle of attack, and the results become the same at 45° angle of attack. The lift coefficient remained the same at 0° and 45° angles of attack, but increased for angles of attack in between.

In the nearly diffuse case with $\alpha = \sigma_\eta = \sigma_\tau = 0.9$, which may represent actual conditions for engineering surfaces at orbital speeds, there were large percentage increases in the lift coefficient (150% to 250%). The actual magnitude of lift coefficients for that

case are quite low (up to 0.17) so the percentage change may be a bit misleading.

The method used for calculating the effects of multiple reflections could enable more accurate results for the calculation of force and moment coefficients on vehicles in low earth orbit. The method of optimization to solve for the defining parameters of the reflected flow could be applied to any type of free molecule calculation scheme, including the more modern and prevalent test particle Monte Carlo method.

REFERENCES

[1]Gazley, C. Jr., Rowell, L.N., and Schilling, G.F., "On the Prediction of Satellite Orbit Decay and Impact," Rand Corporation, Santa Monica California, RM-4619-PR, Oct. 1965.

[2]Kogan, M. N., *Rarefied Gas Dynamics*, Plenum Press, New York, 1969, p. 405.

[3]Patterson, G. N., *Introduction to the Kinetic Theory of Gas Flows*, University of Toronto Press, Toronto, 1971, pg. 59.

[4]Maxwell, J.C., "On Stresses in Rarefied Gases Arising From Inequalities of Temperature," *The Scientific Papers of James Clerk Maxwell*, Vol. 2, Cambridge University Press, Paris, 1890, pp. 681-712.

[5]Loeb, L.B., *The Kinetic Theory of Gases Being a Text and Reference Book Whose Purpose Is to Combine the Classical Deductions with Recent Experimental Advances in a Convenient Form for Student and Investigator*, McGraw-Hill Book Company, New York, 1934, p. 301.

[6]Sänger, E., "The Gas Kinetics of Very High Flight Speeds," NACA, TM 1270, 1950, (translated from 1938 report).

[7]Zahm, A.F., "Superaerodynamics," Journal of the Franklin Institute, Vol. 217, 1934, pp. 153-166.

[8]Tsien, H.S., "Superaerodynamics and Mechanics of Rarefied Gases," *Journal of the Aerospace Sciences*, Vol. 13, 1946, pp. 653-664.

[9]Schaaf, S.A., and Chambré, P.L., "Flow of Rarefied Gases," *Fundamentals of Gas Dynamics*, Princeton University Press, Princeton, New Jersey, 1958, pp. 693-694.

[10]Sentman, L. H., "Free Molecule Flow Theory and Its Application to the Determination of Aerodynamic Forces," LMSC Tech. Rep. 448514, Lockheed Missiles and Space Co., Sunnyvale, California, October 1961.

[11]Warr, J.W., III, "An Orbital Aerodynamics Computer Program to Calculate Force and Moment Coefficients on Complex Vehicle Configurations," Lockheed Missiles & Space Company, Huntsville, Alabama, TM 54/20-275, Aug. 1970.

[12]Cohen, I.M., "Free Molecule Flow Over Non-Convex Bodies," United States Air Force, AFOSR TN 60-190, Report 497, Feb. 1960.

[13]Chahine, M. T., "Free Molecule Flow Over Non-Convex Surfaces," Ph.D. Dissertation, Mechanical Engineering, University of California, January 1961.

[14]Kogan, M. N., *Rarefied Gas Dynamics*, Plenum Press, New York, 1969, p. 420-431.

[15]Patterson, G. N., *Introduction to the Kinetic Theory of Gas Flows*, University of Toronto Press, Toronto, 1971, pp. 106-107.

[16]Bird, G.A., *Molecular Gas Dynamics*, Clarendon Press, Oxford, 1976, pp. 91-106.

[17]Koppenwallner, G., "Freimolekulare Aerodynamik für Satellitenanwendung," [Free Molecular Aerodynamics for Satellite Application,] ESA-TT-776, translated by the European Space Agency, July 1983.

[18]Nocilla, S., "The Surface Re-Emission Law in Free Molecule Flow," *Proceedings of the Third International Symposium on Rarefied Gas Dynamics*, Academic Press, New York, Vol. 1, 1963, pp. 327-346

APPENDIX A: DERIVATION OF THE FITZGERALD EQUATIONS

Determine the distribution function of reflected particles, given an incident stream of particles with a drifting Maxwellian distribution,

$$f_i = \frac{n_i}{(2\pi RT_i)^{3/2}} \exp\left[\frac{-(\xi_i - \underline{U}_i)^2}{2RT_i}\right] \tag{A1}$$

The particles impinge on a surface with known accommodation coefficients, defined as:

$$\alpha = \frac{E_i - |E_r|}{E_i - |E_w|} \quad , \qquad \sigma_n = \frac{P_i - |P_r|}{P_i - |P_w|} \quad , \qquad \sigma_\tau = \frac{\tau_i - |\tau_r|}{\tau_i} \tag{A2}$$

where the fluxes are considered to be scalar quantities. The reflected distribution is assumed to be the drifting Maxwellian distribution, with the unknown parameters of particle speed, direction, and temperature.

$$f_r = \frac{n_r}{(2\pi RT_r)^{3/2}} \exp\left[\frac{-(\xi_r - \underline{U}_r)^2}{2RT_r}\right] \tag{A3}$$

The vector sum of incident and reflected particles is assumed to be zero: $\dot{N}_i + \dot{N}_r = 0$.

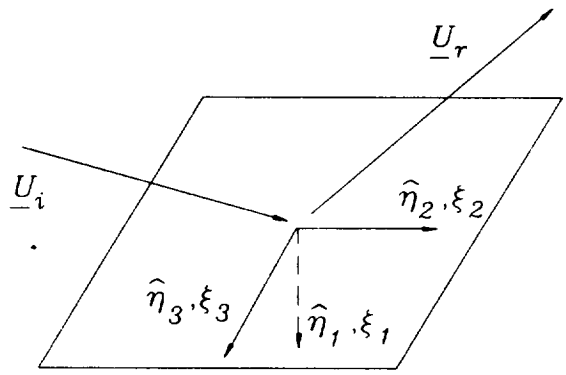

Fig. A1 Geometry and coordinate system for area element.

Define the direction cosines for the velocities in Fig. A1:

$$\psi_i \equiv \frac{\underline{U}_i \cdot \hat{\eta}_1}{|U_i|} \qquad \psi_r \equiv \frac{\underline{U}_r \cdot -\hat{\eta}_1}{|U_r|}$$

$$\phi_i \equiv \frac{\underline{U}_i \cdot \hat{\eta}_2}{|U_i|} \qquad \phi_r \equiv \frac{\underline{U}_r \cdot \hat{\eta}_2}{|U_r|}$$

$$\theta_i \equiv \frac{\underline{U}_i \cdot \hat{\eta}_3}{|U_i|} \qquad \theta_r \equiv \frac{\underline{U}_r \cdot \hat{\eta}_3}{|U_r|}$$

Then the total velocities can be written:

$$\begin{aligned} \underline{\xi}_i &= (\psi_i U_i + c_1)\hat{\eta}_1 + (\phi_i U_i + c_2)\hat{\eta}_2 + (\theta_i U_r + c_3)\hat{\eta}_3 \\ \underline{\xi}_r &= (-\psi_r U_r + c_1)\hat{\eta}_1 + (\phi_r U_r + c_2)\hat{\eta}_2 + (\theta_r U_r + c_3)\hat{\eta}_3 \\ \underline{\xi}_w &= c_1\hat{\eta}_1 + c_2\hat{\eta}_2 + c_3\hat{\eta}_3 \end{aligned} \tag{A4}$$

Or, if the coordinate system has been chosen so that the incident velocity vector is in the $\eta_{1,2}$ plane, then $\theta_i = \theta_r = 0$, and:

$$\underline{\xi}_i = (\psi_i U_i + c_1)\hat{\eta}_1 + (\sqrt{1-\psi_i^2}\,U_i + c_2)\hat{\eta}_2 + c_3\hat{\eta}_3$$

$$\underline{\xi}_r = (-\psi_r U_r + c_1)\hat{\eta}_1 + (\sqrt{1-\psi_r^2}\,U_r + c_2)\hat{\eta}_2 + c_3\hat{\eta}_3$$

$$\underline{\xi}_w = c_1\hat{\eta}_1 + c_2\hat{\eta}_2 + c_3\hat{\eta}_3$$

The number flux of incident particles on a unit area per unit time:

$$\dot{N}_i = \int_0^\infty \int_{-\infty}^\infty \int_{-\infty}^\infty \xi_1 f_i \, d\xi_3 \, d\xi_2 \, d\xi_1$$

$$\dot{N}_i = \frac{n_i}{(2\pi RT_i)^{3/2}} \int_{-\psi_i U_i}^\infty \int_{-\infty}^\infty \int_{-\infty}^\infty (\psi_i U_i + c_1) \exp\left[\frac{-\underline{c}^2}{2RT_i}\right] dc_3 \, dc_2 \, dc_1$$

$$\dot{N}_i = \frac{n_i}{(2\pi RT_i)^{3/2}} \int_{-\psi_i U_i}^\infty (\psi_i U_i + c_1) \exp\left[\frac{-c_1^2}{2RT_i}\right] dc_1 \int_{-\infty}^\infty \exp\left[\frac{-c_2^2}{2RT_i}\right] dc_2 \int_{-\infty}^\infty \exp\left[\frac{-c_3^2}{2RT_i}\right] dc_3$$

After integration, and since $S_i \equiv \dfrac{U_i}{c_{mp}} = \dfrac{U_i}{\sqrt{2RT}}$, and $R = \dfrac{k}{m}$, the particle flux is:

$$\dot{N}_i = n_i\left[\frac{kT_i}{2\pi m}\right]^{1/2}\left[\sqrt{\pi}\,\psi_i S_i(1+\mathrm{erf}\psi_i S_i) + \exp(-\psi_i^2 S_i^2)\right] \tag{A5}$$

For the number flux for all reflected particles:

$$\dot{N}_r = \int_{-\infty}^{0}\int_{-\infty}^{\infty}\int_{-\infty}^{\infty}\xi_1 f_r\, d\xi_3\, d\xi_2\, d\xi_1$$

$$\dot{N}_r = \frac{n_r}{(2\pi RT_r)^{3/2}}\int_{-\infty}^{\psi_r U_r}\int_{-\infty}^{\infty}\int_{-\infty}^{\infty}(-\psi_r U_r + c_1)\exp\left[\frac{-\underline{c}^2}{2RT_r}\right] dc_3\, dc_2\, dc_1$$

$$\dot{N}_r = \frac{n_r}{(2\pi RT_r)^{3/2}}\int_{-\infty}^{\psi_r U_r}(-\psi_r U_r + c_1)\exp\left[\frac{-c_1^2}{2RT_r}\right] dc_1\int_{-\infty}^{\infty}\exp\left[\frac{-c_2^2}{2RT_r}\right] dc_2\int_{-\infty}^{\infty}\exp\left[\frac{-c_3^2}{2RT_r}\right] dc_3$$

After integration and substituting as in (A5), the particle flux is:

$$\dot{N}_r = -n_r\left[\frac{kT_r}{2\pi m}\right]^{1/2}\left[\sqrt{\pi}\,\psi_r S_r(1+\mathrm{erf}\psi_r S_r) + \exp(-\psi_r^2 S_r^2)\right]$$

Substitute into particle conservation and solve for the number density, n_r:

$$n_r = \frac{n_i\left[\frac{kT_i}{2\pi m}\right]^{1/2}\left[\sqrt{\pi}\,\psi_i S_i(1+\mathrm{erf}\psi_i S_i) + \exp(-\psi_i^2 S_i^2)\right]}{\left[\frac{kT_r}{2\pi m}\right]^{1/2}\left[\sqrt{\pi}\,\psi_r S_r(1+\mathrm{erf}\psi_r S_r) + \exp(-\psi_r^2 S_r^2)\right]}$$

$$n_r = n_i\left[\frac{T_i}{T_r}\right]^{1/2}\frac{\sqrt{\pi}\,\psi_i S_i(1+\mathrm{erf}\psi_i S_i) + \exp(-\psi_i^2 S_i^2)}{\sqrt{\pi}\,\psi_r S_r(1+\mathrm{erf}\psi_r S_r) + \exp(-\psi_r^2 S_r^2)} \tag{A6}$$

Number density of particles emitted diffusely from wall:

$$f_w = \frac{n_w}{(2\pi RT_w)^{3/2}}\exp\left[\frac{-\underline{c}^2}{2RT_w}\right]$$

For the case of diffuse emission, $S_w = 0$, since $U_w = 0$, then:

$$n_w = n_i \left(\frac{T_i}{T_w} \right)^{1/2} \left[\sqrt{\pi}\, \psi_i S_i (1 + \mathrm{erf}\psi_i S_i) + \exp(-\psi_i^2 S_i^2) \right] \tag{A7}$$

Pressure due to the flux of particles on an element of surface:

$$P_i = m \int_0^{\infty} \int_{-\infty}^{\infty} \int_{-\infty}^{\infty} \xi_1^2 f_i \, d\xi_3 \, d\xi_2 \, d\xi_1$$

$$P_i = \frac{m n_i}{(2\pi R T_i)^{3/2}} \int_{-\psi_i U_i}^{\infty} \int_{-\infty}^{\infty} \int_{-\infty}^{\infty} (\psi_i U_i + c_1)^2 \exp\left(\frac{-\underline{c}^2}{2RT_i} \right) dc_3 \, dc_2 \, dc_1$$

$$P_i = \frac{m n_i}{(2\pi R T_i)^{3/2}} \int_{-\psi_i U_i}^{\infty} (\psi_i U_i + c_1)^2 \exp\left(\frac{-c_1^2}{2RT_i} \right) dc_1 \int_{-\infty}^{\infty} \exp\left(\frac{-c_2^2}{2RT_i} \right) dc_2 \int_{-\infty}^{\infty} \exp\left(\frac{-c_3^2}{2RT_i} \right) dc_3$$

$$P_i = n_i k T_i \left[(\psi_i^2 S_i^2 + \tfrac{1}{2})(1 + \mathrm{erf}\psi_i S_i) + \frac{\psi_i S_i}{\sqrt{\pi}} \exp(-\psi_i^2 S_i^2) \right] \tag{A8}$$

Resultant pressure from momentum of reflected particles:

$$P_r = m \int_{-\infty}^{0} d\xi_1 \int_{-\infty}^{\infty} d\xi_2 \int_{-\infty}^{\infty} \xi_1 f_r \, d\xi_3$$

$$P_r = \frac{m n_r}{(2\pi R T_r)^{3/2}} \int_{-\infty}^{\psi_r U_r} \int_{-\infty}^{\infty} \int_{-\infty}^{\infty} (\psi_r U_r + c_1)^2 \exp\left(\frac{-\underline{c}^2}{2RT_r} \right) dc_3 \, dc_2 \, dc_1$$

$$P_r = \frac{m n_r}{(2\pi R T_r)^{3/2}} \int_{-\infty}^{\psi_r U_r} (\psi_r U_r + c_1)^2 \exp\left(\frac{-c_1^2}{2RT_r} \right) dc_1 \int_{-\infty}^{\infty} \exp\left(\frac{-c_2^2}{2RT_r} \right) dc_2 \int_{-\infty}^{\infty} \exp\left(\frac{-c_3^2}{2RT_r} \right) dc_3$$

$$P_r = n_r k T_r \left[(\psi_r^2 S_r^2 + \tfrac{1}{2})(1 + \mathrm{erf}\psi_r S_r) + \frac{\psi_r S_r}{\sqrt{\pi}} \exp(-\psi_r^2 S_r^2) \right] \tag{A9}$$

Pressure due to diffusely emitted particles:

$$P_w = m \int_{-\infty}^{0} d\xi_1 \int_{-\infty}^{\infty} d\xi_2 \int_{-\infty}^{\infty} \xi_1^2 f_w \, d\xi_3$$

$$P_w = \frac{m n_w}{(2\pi R T_w)^{3/2}} \int_{-\infty}^{0} \int_{-\infty}^{\infty} \int_{-\infty}^{\infty} c_1^2 \exp\left(\frac{-\underline{c}^2}{2RT_w} \right) dc_3 \, dc_2 \, dc_1$$

$$P_w = \frac{mn_w}{(2\pi RT_w)^{3/2}} \int_{-\infty}^{0} c_1^2 \exp\left[\frac{-c_1^2}{2RT_w}\right] dc_1 \int_{-\infty}^{\infty} \exp\left[\frac{-c_2^2}{2RT_w}\right] dc_2 \int_{-\infty}^{\infty} \exp\left[\frac{-c_3^2}{2RT_w}\right] dc_3$$

$$P_w = \frac{n_w k T_w}{2} \tag{A10}$$

Shear stresses at the surface due to incident flow:

$$\tau_{\eta_{2_i}} = m \int_0^{\infty} \int_{-\infty}^{\infty} \int_{-\infty}^{\infty} \xi_1 \xi_2 f_i \, d\xi_3 \, d\xi_2 \, d\xi_1$$

$$\tau_{\eta_{2_i}} = \frac{mn_i}{(2\pi RT_i)^{3/2}} \int_{-\psi_i U_i}^{\infty} \int_{-\infty}^{\infty} \int_{-\infty}^{\infty} (\psi_i U_i + c_1)(\phi_i U_i + c_2) \exp\left[\frac{-\underline{c}^2}{2RT_i}\right] dc_3 \, dc_2 \, dc_1$$

$$\tau_{\eta_{2_i}} = \frac{mn_i}{(2\pi RT_i)^{3/2}} \int_{-\infty}^{\infty} \exp\left[\frac{-c_3^2}{2RT_i}\right] dc_3 \int_{-\psi_i U_i}^{\infty} \exp\left[\frac{-c_1^2}{2RT_i}\right] \times$$

$$\int_{-\infty}^{\infty} (\psi_i \phi_i U_i^2 + c_1 \phi_i U_i + c_2 \phi_i U_i + c_1 c_2) \exp\left[\frac{-c_2^2}{2RT_i}\right] dc_2 \, dc_1$$

$$\tau_{\eta_{2_i}} = n_i k T_i \phi_i \left[\psi_i S_i^2 (1 + \operatorname{erf} \psi_i S_i) + \frac{S_i}{\sqrt{\pi}} \exp(-\psi_i^2 S_i^2)\right]$$

and $\tau_{\eta_{3_i}} = 0$, since $\theta_i = 0$

If a substitution is made for $\phi_i = \sqrt{1-\psi_i^2}$, then:

$$\tau_i = n_i k T_i (1-\psi_i^2)^{1/2} \left[\psi_i S_i^2 (1 + \operatorname{erf} \psi_i S_i) + \frac{S_i}{\sqrt{\pi}} \exp(-\psi_i^2 S_i^2)\right] \tag{A11}$$

Shear stresses due to reflected particles:

$$\tau_{\eta_{2_r}} = m \int_{-\infty}^{0} \int_{-\infty}^{\infty} \int_{-\infty}^{\infty} \xi_1 \xi_2 f_r \, d\xi_3 \, d\xi_2 \, d\xi_1$$

$$\tau_{\eta_{2_r}} = \frac{mn_r}{(2\pi RT_r)^{3/2}} \int_{\infty}^{\psi_r U_r} \int_{-\infty}^{\infty} \int_{-\infty}^{\infty} (-\psi_r U_r + c_1)(\phi_r U_r + c_2) \exp\left[\frac{-\underline{c}^2}{2RT_r}\right] dc_3 \, dc_2 \, dc_1$$

$$\tau_{\eta_{2_r}} = \frac{mn_r}{(2\pi RT_r)^{3/2}} \int_{-\infty}^{\infty} \exp\left[\frac{-c_3^2}{2RT_r}\right] dc_3 \int_{-\infty}^{\psi_r U_r} \exp\left[\frac{-c_1^2}{2RT_r}\right] \times$$

$$\int_{-\infty}^{\infty} (-\psi_r \phi_r U_r^2 + c_1 \phi_r U_r - c_2 \phi_r U_r + c_1 c_2) \exp\left[\frac{-c_2^2}{2RT_r}\right] dc_2\, dc_1$$

$$\tau_{\eta_{2_r}} = -n_r k T_r \phi_r \left[\psi_r S_r^2 (1 + \text{erf}\psi_r S_r) + \frac{S_r}{\sqrt{\pi}} \exp(-\psi_r^2 S_r^2)\right]$$

and $\tau_{\eta_{3_r}} = 0$, since $\theta_r = 0$

If a substitution is made for $\phi_r = \sqrt{1-\psi_r^2}$, then:

$$\tau_r = -n_r k T_r (1-\psi_r^2)^{1/2} \left[\psi_r S_r^2 (1 + \text{erf}\psi_r S_r) + \frac{S_r}{\sqrt{\pi}} \exp(-\psi_r^2 S_r^2)\right] \qquad \text{(A12)}$$

For diffusely emitted particles, since $S_w = 0$, there is no contribution to the shear forces:

$$\tau_w = \tau_{\eta_{2_w}} = \tau_{\eta_{3_w}} = 0 \qquad \text{(A13)}$$

For the flux of incident energy at the surface, the internal energy for each degree of freedom (DOF) is $\frac{1}{2}kT_i$. For a perfect gas, DOF $= \frac{5-3\gamma}{\gamma-1}$. The incident energy flux is:

$$E_i = \int_0^{\infty} \int_{-\infty}^{\infty} \int_{-\infty}^{\infty} \xi_1 \left[\frac{1}{2} m\xi^2 + \frac{kT_i}{2}\left(\frac{5-3\gamma}{\gamma-1}\right)\right] f_i d\xi_3 d\xi_2 d\xi_1$$

$$E_i = \frac{m}{2} \int_0^{\infty} \int_{-\infty}^{\infty} \int_{-\infty}^{\infty} \xi_1 \xi^2 f_i d\xi_3 d\xi_2 d\xi_1 + \frac{kT_i}{2}\left(\frac{5-3\gamma}{\gamma-1}\right) \int_0^{\infty} \int_{-\infty}^{\infty} \int_{-\infty}^{\infty} \xi_1 f_i d\xi_3 d\xi_2 d\xi_1$$

The second term, internal energy, is equal to $\dot{N}_i \frac{kT_i}{2}\left(\frac{5-3\gamma}{\gamma-1}\right)$, or:

$$E_{INT_i} = \frac{n_i k T_i}{2}\left(\frac{kT_i}{2\pi m}\right)^{1/2}\left[\sqrt{\pi}\,\psi_i S_i(1+\mathrm{erf}\psi_i S_i) + \exp(-\psi_i^2 S_i^2)\right]\left(\frac{5-3\gamma}{\gamma-1}\right) \tag{A14}$$

$$E_i = \frac{mn_i}{2(2\pi RT_i)^{3/2}}\int_{-\psi_i U_i}^{\infty}\int_{-\infty}^{\infty}\int_{-\infty}^{\infty}(\psi_i U_i + c_1)(U_i^2 + 2c_1U_i\psi_i + 2c_2U_i\sqrt{1-\psi_i^2} + c_1^2 + c_2^2 + c_3^2) \times \exp\left(\frac{-\underline{c}^2}{2RT_i}\right) dc_3 dc_2 dc_1 + E_{INT_i}$$

$$E_i = n_i k T_i\left(\frac{kT_i}{2\pi m}\right)^{1/2}\left[\sqrt{\pi}\,\psi_i S_i(S_i^2+\frac{5}{2})(1+\mathrm{erf}\psi_i S_i) + (S_i^2+2)\exp(-\psi_i^2 S_i^2)\right] + E_{INT_i} \tag{A15}$$

The flux of energy from all the reflected particles is:

$$E_r = \int_{-\infty}^{0}\int_{-\infty}^{\infty}\int_{-\infty}^{\infty}\xi_1\left[\frac{1}{2}m\underline{\xi}^2 + \frac{kT_r}{2}\left(\frac{5-3\gamma}{\gamma-1}\right)\right] f_r d\xi_3 d\xi_2 d\xi_1$$

$$E_r = \frac{m}{2}\int_{-\infty}^{0}\int_{-\infty}^{\infty}\int_{-\infty}^{\infty}\xi_1\xi^2 f_r d\xi_3 d\xi_2 d\xi_1 + \frac{kT_r}{2}\left(\frac{5-3\gamma}{\gamma-1}\right)\int_{-\infty}^{0}\int_{-\infty}^{\infty}\int_{-\infty}^{\infty}\xi_1 f_r d\xi_3 d\xi_2 d\xi_1$$

The second term is internal energy as before, $\dot{N}_r\frac{kT_r}{2}\left(\frac{5-3\gamma}{\gamma-1}\right)$, or:

$$E_{INT_r} = \frac{-n_r k T_r}{2}\left(\frac{kT_r}{2\pi m}\right)^{1/2}\left[\sqrt{\pi}\,\psi_r S_r(1+\mathrm{erf}\psi_r S_r) + \exp(-\psi_r^2 S_r^2)\right]\left(\frac{5-3\gamma}{\gamma-1}\right) \tag{A16}$$

$$E_r = \frac{mn_r}{2(2\pi RT_r)^{3/2}}\int_{-\infty}^{\psi_r U_r}\int_{-\infty}^{\infty}\int_{-\infty}^{\infty}(-\psi_r U_r + c_1)(U_r^2 - 2c_1U_r\psi_r + 2c_2U_r\sqrt{1-\psi_r^2} + c_1^2 + c_2^2 + c_3^2) \times \exp\left(\frac{-\underline{c}^2}{2RT_r}\right) dc_3 dc_2 dc_1 + E_{INT_r}$$

$$E_r = -n_r k T_r\left(\frac{kT_r}{2\pi m}\right)^{1/2}\left[\sqrt{\pi}\,\psi_r S_r(S_r^2+\tfrac{5}{2})(1+\mathrm{erf}(\psi_r S_r)) + (S_r^2+2)\exp(-\psi_r^2 S_r^2)\right] + E_{INT_r} \tag{A17}$$

The energy flux from a surface element with diffuse emission:

$$E_w = \int_{-\infty}^{0}\int_{-\infty}^{\infty}\int_{-\infty}^{\infty}\xi_1\left[\frac{1}{2}m\xi^2 + \frac{kT_w}{2}\left(\frac{5-3\gamma}{\gamma-1}\right)\right]f_w d\xi_3 d\xi_2 d\xi_1$$

$$E_w = \frac{m}{2}\int_{-\infty}^{0}\int_{-\infty}^{\infty}\int_{-\infty}^{\infty}\xi_1\xi^2 f_w d\xi_3 d\xi_2 d\xi_1 + \frac{kT_w}{2}\left(\frac{5-3\gamma}{\gamma-1}\right)\int_{-\infty}^{0}\int_{-\infty}^{\infty}\int_{-\infty}^{\infty}\xi_1 f_w d\xi_3 d\xi_2 d\xi_1$$

where the internal energy term is $\dot{N}_w\frac{kT_w}{2}\left(\frac{5-3\gamma}{\gamma-1}\right)$, and since $S_w = 0$:

$$E_{INT_w} = \frac{-n_w kT_w}{2}\left(\frac{kT_w}{2\pi m}\right)^{1/2}\left(\frac{5-3\gamma}{\gamma-1}\right) \tag{A18}$$

$$E_w = \frac{mn_w}{2(2\pi RT_w)^{3/2}}\int_{-\infty}^{0}\int_{-\infty}^{\infty}\int_{-\infty}^{\infty}c_1(c_1^2+c_2^2+c_3^2)\exp\left(\frac{-\underline{c}^2}{2RT_r}\right)dc_3 dc_2 dc_1 + E_{INT_w}$$

$$E_w = -2\,n_w kT_w\left(\frac{kT_w}{2\pi m}\right)^{1/2} + E_{INT_w}$$

$$E_w = -n_w kT_w\left(\frac{kT_w}{2\pi m}\right)^{1/2}\left(\frac{\gamma+1}{2(\gamma-1)}\right) \tag{A19}$$

Create a set of equations to solve for the desired quantities T_r, S_r, ψ_r. Rearrange accommodation expressions, (A2), and set equal to zero.

$$F_1 = 0 = (1-\sigma_\tau)\tau_i - |\tau_r|$$

$$F_2 = 0 = (1-\sigma_n)P_i + \sigma_n|P_w| - |P_r|$$

$$F_3 = 0 = (1-\alpha)E_i + \alpha|E_w| - |E_r|$$

Substituting (A11) and (A12) into F_1:

$$F_1 = (1-\sigma_\tau)n_i kT_i(1-\psi_i^2)^{1/2}\left[\psi_i S_i^2(1+\mathrm{erf}\psi_i S_i) + \frac{S_i}{\sqrt{\pi}}\exp(-\psi_i^2 S_i^2)\right] -$$
$$n_r kT_r(1-\psi_r^2)^{1/2}\left[\psi_r S_r^2(1+\mathrm{erf}\psi_r S_r) + \frac{S_r}{\sqrt{\pi}}\exp(-\psi_r^2 S_r^2)\right]$$

Or, after substituting (A6) for n_r and simplifying:

$$F_1 = 0 = (1-\sigma_r)S_i[T_i(1-\psi_i^2)]^{1/2} - S_r[T_r(1-\psi_r^2)]^{1/2} \tag{A20}$$

To make the expressions more concise, define the quantity:

$$\chi(\psi,S) = \sqrt{\pi}\,\psi S(1+\mathrm{erf}\psi S) + \exp(-\psi^2 S^2) \tag{A21}$$

Substituting (A8), (A9), (A10), and (A21) into F_2:

$$F_2 = (1-\sigma_n)\frac{n_i kT_i}{\sqrt{\pi}}\left[\frac{\sqrt{\pi}}{2}(1+\mathrm{erf}\psi_i S_i) + \psi_i S_i \chi(\psi_i,S_i)\right] + \sigma_n \frac{n_w kT_w}{2} - \frac{n_r kT_r}{\sqrt{\pi}}\left[\frac{\sqrt{\pi}}{2}(1+\mathrm{erf}\psi_r S_r) + \psi_r S_r \chi(\psi_r,S_r)\right]$$

Substituting (A6) for n_r and simplifying:

$$F_2 = (1-\sigma_n)\left[\frac{\sqrt{\pi T_i}}{2}\frac{(1+\mathrm{erf}\psi_i S_i)}{\chi(\psi_i,S_i)} + \sqrt{T_i}\,\psi_i S_i\right] + \sigma_n \frac{\sqrt{\pi T_w}}{2} - \left[\frac{\sqrt{\pi T_i}}{2}\frac{(1+\mathrm{erf}\psi_r S_r)}{\chi(\psi_r,S_r)} + \sqrt{T_r}\,\psi_r S_r\right] \tag{A22}$$

Substituting (A14), (A15), (A16), (A17), (A18), (A19), and (A21) into F_3:

$$F_3 = (1-\alpha)n_i kT_i\left[\frac{kT_i}{2\pi m}\right]^{1/2}\left[\frac{\sqrt{\pi}}{2}\psi_i S_i(1+\mathrm{erf}\psi_i S_i)+(S_i^2+2)\chi(\psi_i,S_i) + \left[\frac{5-3\gamma}{2(\gamma-1)}\right]\chi(\psi_i,S_i)\right] + \alpha n_w kT_w\left[\frac{kT_w}{2\pi m}\right]^{1/2}\left[\frac{\gamma+1}{2(\gamma-1)}\right] - n_r kT_r\left[\frac{kT_r}{2\pi m}\right]^{1/2}\left[\frac{\sqrt{\pi}}{2}\psi_r S_r(1+\mathrm{erf}\psi_r S_r)+(S_r^2+2)\chi(\psi_r,S_r) + \left[\frac{5-3\gamma}{2(\gamma-1)}\right]\chi(\psi_r,S_r)\right]$$

Or, after substituting (A6) for n_r and simplifying:

$$F_3 = (1-\alpha)T_i\left[\frac{\sqrt{\pi}\psi_i S_i}{2}\frac{(1+\mathrm{erf}\psi_i S_i)}{\chi(\psi_i,S_i)} + (S_i^2+2) + \frac{5-3\gamma}{2(\gamma-1)}\right] + \alpha T_w\left[\frac{\gamma+1}{2(\gamma-1)}\right] - T_r\left[\frac{\sqrt{\pi}\psi_r S_r}{2}\frac{(1+\mathrm{erf}\psi_r S_r)}{\chi(\psi_r,S_r)} + (S_r^2+2) + \frac{5-3\gamma}{2(\gamma-1)}\right] \quad \text{(A23)}$$

Form an objective function from F_1, F_2, F_3:

$$J = \frac{1}{2}\left[F_1^2 + F_2^2 + F_3^2\right] \quad \text{(A24)}$$

The objective or "cost" function can be solved by a nonlinear optimization technique. J can be minimized given the input values of σ_n, σ_r, α, T_i, ψ_i, S_i, γ, and T_w. These quantities are known from material properties, atmospheric data and the geometry of the problem. Minimization results in the desired values of ψ_r, S_r, and T_r necessary for the determination of the distribution of the stream reflected from a surface.

APPENDIX B: VERIFICATION OF REFLECTED FLOW PROPERTIES

After experimenting with the optimization process to determine the properties of the reflected flow from a surface, it was apparent that choosing a random set of accommodation coefficients for energy and momentum would not insure a correct solution. There were apparently certain "sets" of accommodation coefficients that could yield correct solutions. Two issues needed an answer. The first was whether or not the reflected properties from the minimization were an adequate solution to the set of equations. The second was whether or not the solution was reasonable or even physically possible.

To determine if the minimization was finding global minimums in the solution of the set of conservation equations, the value of the cost function itself could be monitored. A series of tests were carried out with the optimization program to try various combinations of accommodation and find out what the cost function looked like. A set of input conditions was chosen and a fixed energy accommodation value was selected. The tangential and normal momentum accommodation coefficients were then cycled through 0.0 to 1.0, and a surface of the cost function was generated. From the cost surface and for each value of energy accommodation, a region of normal and tangential accommodation that produced a low cost function could be determined. For this purpose, any solution that produced a cost value of 10^{-4} or less was considered to be an adequate solution.

If the optimized reflected quantities could be compared to another known solution to the problem, it could be determined if the solution was physically reasonable. In gas kinetics, there is an expression for the pressure due to the stream of gas particles reflected from a surface. Using the reflected distribution:

$$P_{r_1} = \frac{T_r}{\sqrt{\pi}}\left[\psi_r S_r \exp(-\psi_r^2 S_r^2) + \sqrt{\pi}(\psi_r^2 S_r^2 + \tfrac{1}{2})(1 + \operatorname{erf}\psi_r S_r)\right]$$
$$\sqrt{\frac{T_i}{T_r}}\frac{\left[\exp(-\psi_i^2 S_i^2) + \sqrt{\pi}\psi_i S_i(1 + \operatorname{erf}\psi_i S_i)\right]}{\left[\exp(-\psi_r^2 S_r^2) + \sqrt{\pi}\psi_r S_r(1 + \operatorname{erf}\psi_r S_r)\right]} \qquad \text{(B1)}$$

There is also an expression that calculates the resultant pressure of the reflected flow using the incident and wall conditions and accommodation coefficients. The resultant pressure, using the accommodation method:

$$P_i = \frac{T_i}{\sqrt{\pi}}\left[\psi_i S_i \exp(-\psi_i^2 S_i^2) + \sqrt{\pi}(\psi_i^2 S_i^2 + \tfrac{1}{2})(1 + \operatorname{erf}\psi_i S_i)\right]$$
$$P_w = \frac{T_w}{2}\sqrt{\frac{T_i}{T_w}}\left[\exp(-\psi_i^2 S_i^2) + \sqrt{\pi}\psi_i S_i(1 + \operatorname{erf}\psi_i S_i)\right] \qquad \text{(B2)}$$
$$P_{r_2} = (1 - \sigma_n)P_i + \sigma_n P_w$$

where both pressure expressions have been divided by $n_i k$ to simplify the expressions. By looking at a surface generated by the ratio of the pressures, P_{r1}/P_{r2}, a contour where the pressure ratio is 1.0 can be picked out.

To get an idea if the optimization was producing valid answers for the reflected properties, the regions of low cost function were overlaid with the contour of unit pressure ratios. Figures B1 through B9 show the correspondence between the regions of low cost function and the unit pressure ratio for an incidence angle of 20°.

Several things can be learned from the results. There is evidence that the accommodation coefficients may actually be a function of the angle of incidence of the impinging flow, as suggested by several investigators. For the cases with a 20° angle

between the surface normal and flow in Figs. B1 through B3, the tangential momentum accommodation coefficient does not seem significant, but the normal accommodation takes on a small range of values, linked to the energy accommodation.

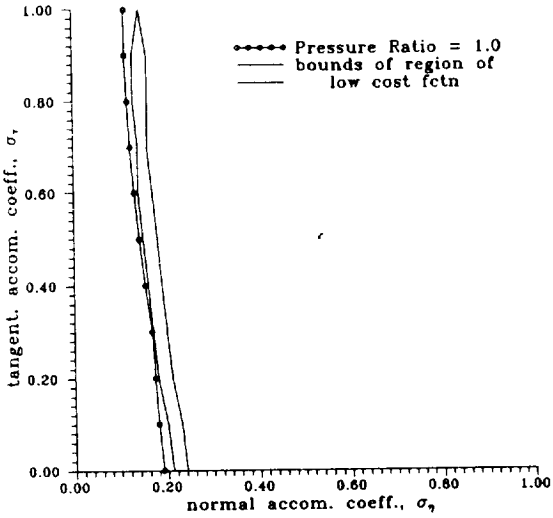

Fig. B1 Unit pressure ratios and region of low cost function for $\alpha = 0.3$, $\theta_i = 20^\circ$, $S_i = 8.$, and $T_w/T_i = 0.25$.

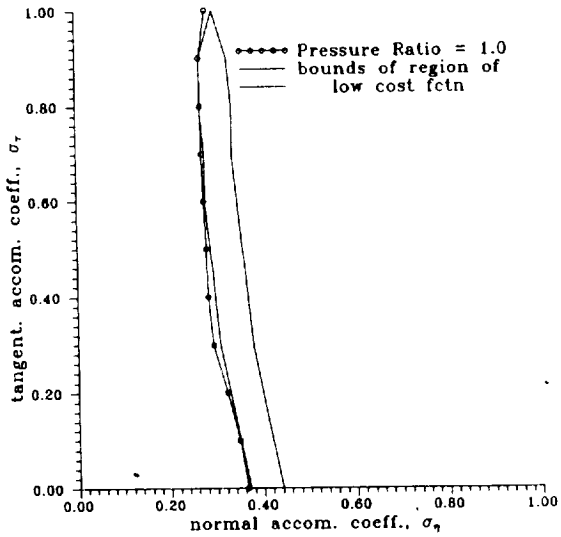

Fig. B2 Unit pressure ratios and region of low cost function for $\alpha = 0.5$, $\theta_i = 20^\circ$, $S_i = 8.$, and $T_w/T_i = 0.25$.

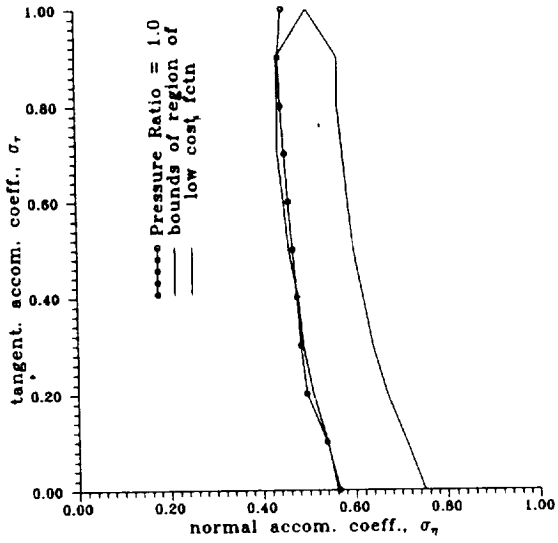

Fig. B3 Unit pressure ratios and region of low cost function for $\alpha = 0.7$, $\theta_i = 20^\circ$, $S_i = 8.$, and $T_w/T_i = 0.25$.

The cases with an incidence angle of 45° in Figs. B4 through B6 show that the normal and tangential accommodation are both nearly equally significant. Again, the energy accommodation is linked to the range of momentum accommodation values that are "possible".

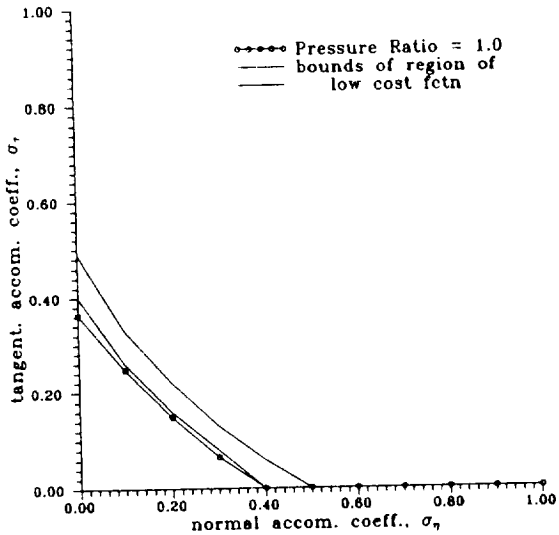

Fig. B4 Unit pressure ratios and region of low cost function for $\alpha = 0.3$, $\theta_i = 45°$, $S_i = 8.$, and $T_w/T_i = 0.25$.

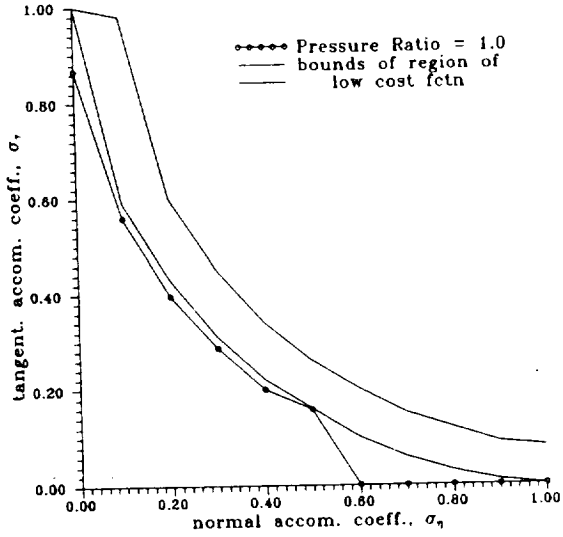

Fig. B5 Unit pressure ratios and region of low cost function for $\alpha = 0.5$, $\theta_i = 45°$, $S_i = 8.$, and $T_w/T_i = 0.25$.

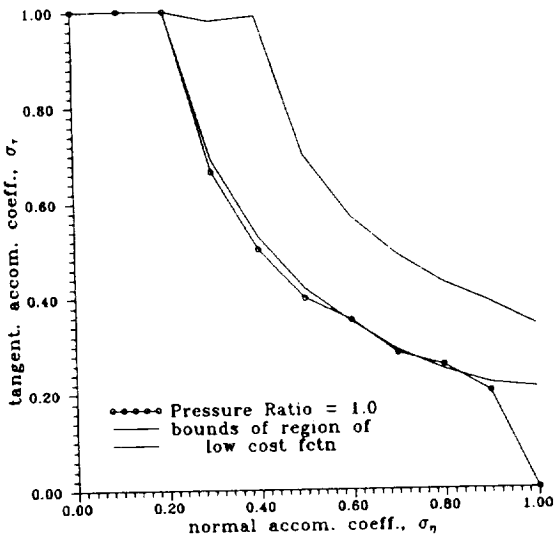

Fig. B6 Unit pressure ratios and region of low cost function for $\alpha = 0.7$, $\theta_i = 45^\circ$, $S_i = 8.$, and $T_w/T_i = 0.25$.

Figures B7 through B9 show the regions of low cost function and pressure ratio of 1.0 for an incidence angle of 70°. The results are similar to the 20° case in that the component of momentum in a direction that is not close to the incident flow is not as significant as the momentum direction that is closer to the incident direction.

To choose a set of accommodation coefficients for this investigation, it was desired to have accommodation values that would stay in the low cost region for the entire range of angles of attack. It was found that an adequate set of accommodation coefficients would likely have nearly equal tangential and normal momentum accommodation, and an energy accommodation coefficient that was slightly greater than the momentum values.

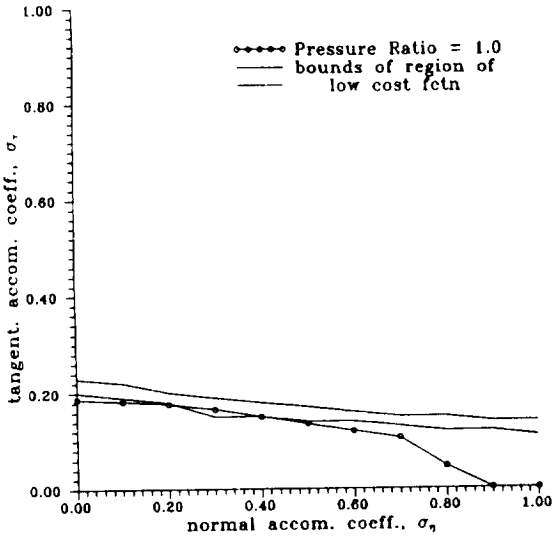

Fig. B7 Unit pressure ratios and region of low cost function for $\alpha = 0.3$, $\theta_i = 70^\circ$, $S_i = 8.$, and $T_w/T_i = 0.25$.

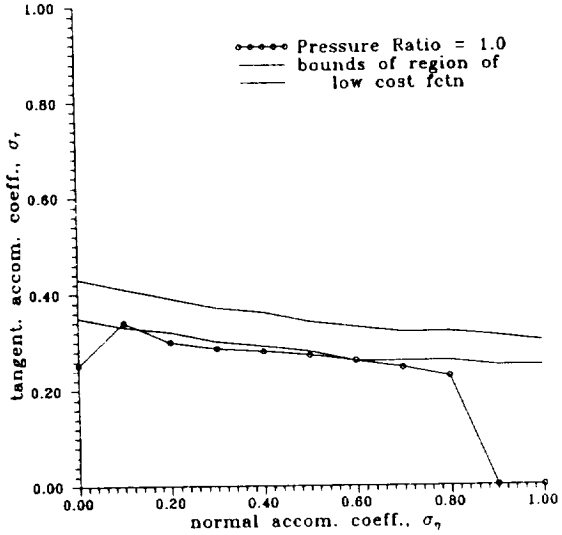

Fig. B8 Unit pressure ratios and region of low cost function for $\alpha = 0.5$, $\theta_i = 70^\circ$, $S_i = 8.$, and $T_w/T_i = 0.25$.

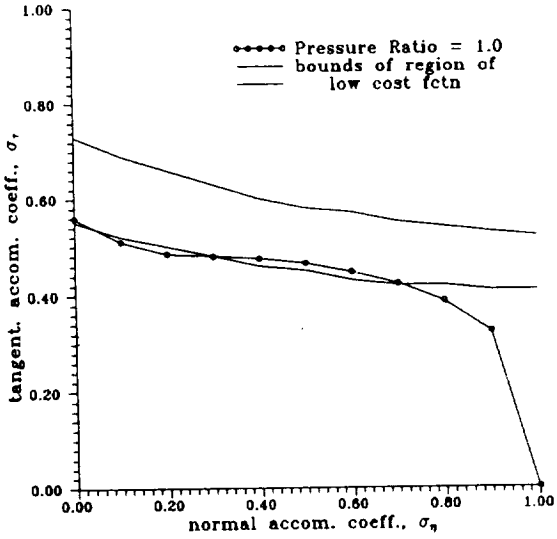

Fig. B9 Unit pressure ratios and region of low cost function for $\alpha = 0.7$, $\theta_i = 70^\circ$, $S_i = 8.$, and $T_w/T_i = 0.25$.

VITA

Gordon Lee Powell, Jr. was born [redacted] to Mr. Gordon Powell, Sr. and Mrs. Mary Powell. He lived there until he graduated from high school at La Crosse Central in 1985. Gordon was offered a Lechner Fellowship to study engineering at Texas A&M University, so headed south. He attended school in Texas and worked back in La Crosse during the summers to help fund the completion of his Bachelor of Science degree in Aerospace Engineering in 1989. Gordon worked for the Aerospace Engineering Department as a research assistant under a NASA JSC contract, then worked for the Center for Strategic Technology, headed by Dr. Richard E. Thomas. He continued to work for Dr. Thomas as a research assistant for R. Thomas and Associates. Gordon was president of the Texas A&M University Bicycling Club for over five years, before becoming a student advisor to the club during his last few semesters at A&M. After the completion of his Master of Science degree, Gordon intends to embark on the greatest adventure of his life--the search for full time employment. Gordon can be reached through his parents at: [redacted]